



UNIVERSIDADE FEDERAL DE PELOTAS
Pró-Reitoria de Pesquisa, Pós-Graduação e Inovação
Centro de Ciências Químicas, Farmacêuticas e de Alimentos
Programa de Pós-Graduação em Química

EDITAL Nº 45/2021

SELEÇÃO DE ALUNO REGULAR 2021/01-02

Programa recomendado pela CAPES, nível Mestrado, em 12 de julho de 2006.

Programa recomendado pela CAPES, nível Doutorado, em 1º de março de 2011.

No artigo selecionado, estão presentes questões que nos permitem analisar a Química em sua área básica. Neste caso, uma análise sobre a formação de interações intermoleculares, fatores que afetam a cristalização de materiais, o efeito do solvente no favorecimento de certos tipos de interações e/ou formação de novas ligações e seu efeito em sistemas automontados, pode ser observada. Além disso, para corroborar com os resultados, técnicas experimentais consolidadas na química e parâmetros quantitativos são empregados para caracterizar os materiais formados, além de considerar questões acerca de efeitos termodinâmicos e cinéticos sobre as interações intermoleculares.

Com base nessas características do artigo, elabore um documento, seguindo formatação típica de um artigo científico, que articule em um texto coerente os seguintes pontos:

- i) Um panorama geral do artigo utilizado como indutor das discussões;
- ii) Uma discussão a respeito de interações intermoleculares, articulada com as questões destacadas no artigo, e que aborde aspectos:
 - a. Relacionados a conceitos básicos associados às interações intermoleculares;
 - b. Referentes aos impactos, aplicações e potencialidades na área de Química.
- iii) Relações entre o texto e o cenário recente da pesquisa em Química e suas subáreas, além de articulações com outros textos do campo da Química e áreas afins.

Uma boa prova!

Supplementary Information

Hydrogen bonding vs halogen bonding: the solvent decides

Craig C. Robertson,¹ James S. Wright,¹ Elliot J. Carrington,^{1,†} Robin N. Perutz*,² Christopher A. Hunter*,³ and Lee Brammer*,¹

¹ Department of Chemistry, University of Sheffield, Sheffield, S3 7HF, UK

² Department of Chemistry, University of York, Heslington, York, YO10 5DD, UK

³ Department of Chemistry, Lensfield Road, University of Cambridge, Cambridge, CB2 1EW, UK

[†] Current address: Department of Chemistry, University of Liverpool, Liverpool L69 7ZD, UK.

Contents

| | |
|---|----------|
| 1. General Experimental | page S2 |
| 2. Procedure for NMR titrations | page S2 |
| 3. Table of Association Constants | page S3 |
| 4. Spectra and Binding Isotherms of Titrations | page S4 |
| 5. Synthesis of Co-crystals | page S14 |
| 6. Full Table of Powder X-ray Diffraction Results | page S16 |
| 7. Phase Purity Analysis by XRPD: Experimental Description | page S16 |
| 8. Phase Purity Checks by XRPD: Compounds 1 , 2a , 2b , 2c and 3 | page S17 |
| 9. Phase Purity Check by XRPD: Co-crystals 1•3 , 2a•3 , 2b•3 and 2c•3 | page S22 |
| 10. Determination of Product Composition by XRPD: System A | page S26 |
| 11. Determination of Product Composition by XRPD: System B | page S33 |
| 12. Determination of Product Composition by XRPD: System C | page S40 |
| 13. Single Crystal Diffraction Studies | page S45 |
| 14. References | page S46 |

1. General Experimental

Chemicals and Spectroscopic Grade Solvents were purchased from Alfa Aesar, Apollo Scientific Ltd, Fisher Scientific UK Ltd., Fluorochem Ltd, Sigma–Aldrich Company Ltd. or VWR International Ltd and used without further purification.

^1H and ^{19}F NMR spectra were recorded on a Bruker Avance II 400 spectrometer at 400.1 MHz and 374.9 Hz respectively, using the deuterated solvent or a capillary insert with D_2O as the lock. In the assignment of ^1H NMR spectra, the chemical shift (δH) for each resonance is given in units of parts per million (ppm) relative to trimethylsilane (TMS) where $\delta\text{H TMS} = 0.00$ ppm.

In the assignment of ^{19}F NMR spectra, the chemical shift (δF) for each resonance is given in units of parts per million (ppm) relative to CFCl_3 where $\delta\text{F CFCl}_3 = 0.00$ ppm.

Analyses of NMR spectra were carried out using Topspin version 3.2 or iNMR version 5.2.1.

Measurement of mass of solids was carried out on a Precisa 125A balance.

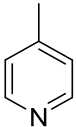
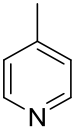
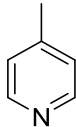
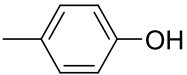
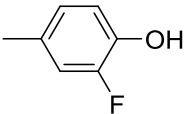
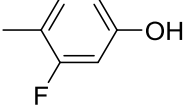
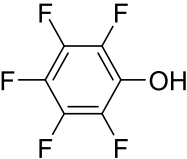
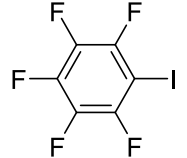
Measurement of volumes of liquids for the preparation of samples for NMR titrations was carried out using Eppendorf Multipette XStream electronic pipettors.

2. Procedure for NMR titrations

10 NMR Norell S-400 tubes, each with different concentrations of host and guest as measured with a programmed Multipette XStream were set up and submitted to BACS automated sample recording. The concentration of guest was chosen to obtain a binding isotherm of >50% saturation in each titration. The specific concentration of guest used in each experiment can be seen in the horizontal axis of the binding isotherm for each titration shown below. Titrations were repeated at least twice for reproducibility and estimation of errors. K_a data were obtained by fitting the experimental results to a binding isotherm using a macro-based Microsoft Excel fitting program written by Christopher A. Hunter (University of Cambridge).

3. Table of Association Constants

Table S1. Association constants (K_a) and errors*

| Solvent | Toluene (α_s 1.0; β_s 2.1) | Chloroform (α_s 2.2; β_s 0.8) | Acetonitrile (α_s 1.8; β_s 5.1) |
|---|---|---|---|
| Guest |  |  |  |
| Host | | | |
|  | 31±1 | 19±2 | <1 |
|  | 40±1 | 20±1 | <1 |
|  | 62±5 | 52±2 | <1 |
|  | 1300±50 | 850±60 | 19±1 |
|  | 1±1 | <1 | <1 |

*Errors determined by $2 \times$ standard deviation of multiple repeat titrations

4. Spectra and binding isotherms of titrations

Titration of *p*-cresol with 4-picoline in Toluene

Host: *p*-cresol [18.4 mM]

Guest: 4-picoline

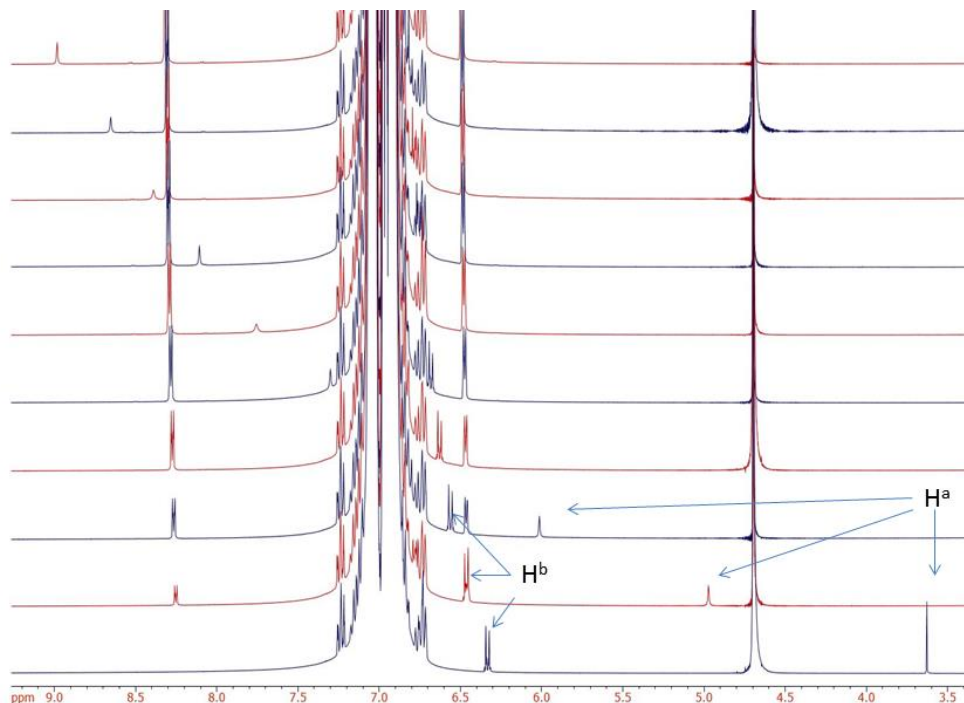


Figure S4.1: partial 400.2 MHz ^1H NMR spectra of titration in toluene with monitored signals labelled.

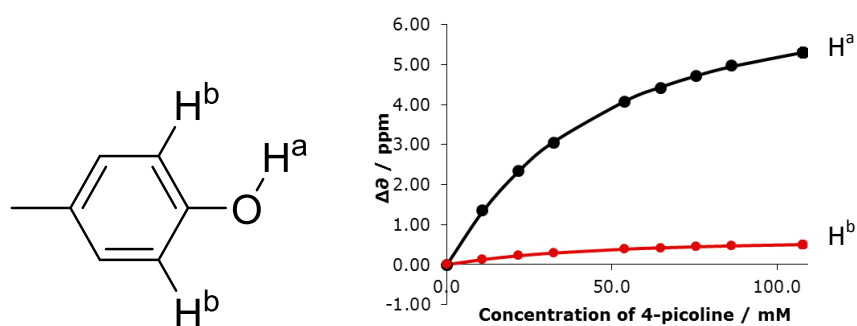


Figure S4.2: Binding isotherms for titration

$$K_a = 31 \pm 1 \text{ M}^{-1} \quad 74\% \text{ bound}$$

Titration of *p*-cresol with 4-picoline in chloroform

Host: *p*-cresol [11.5 mM]

Guest: 4-picoline

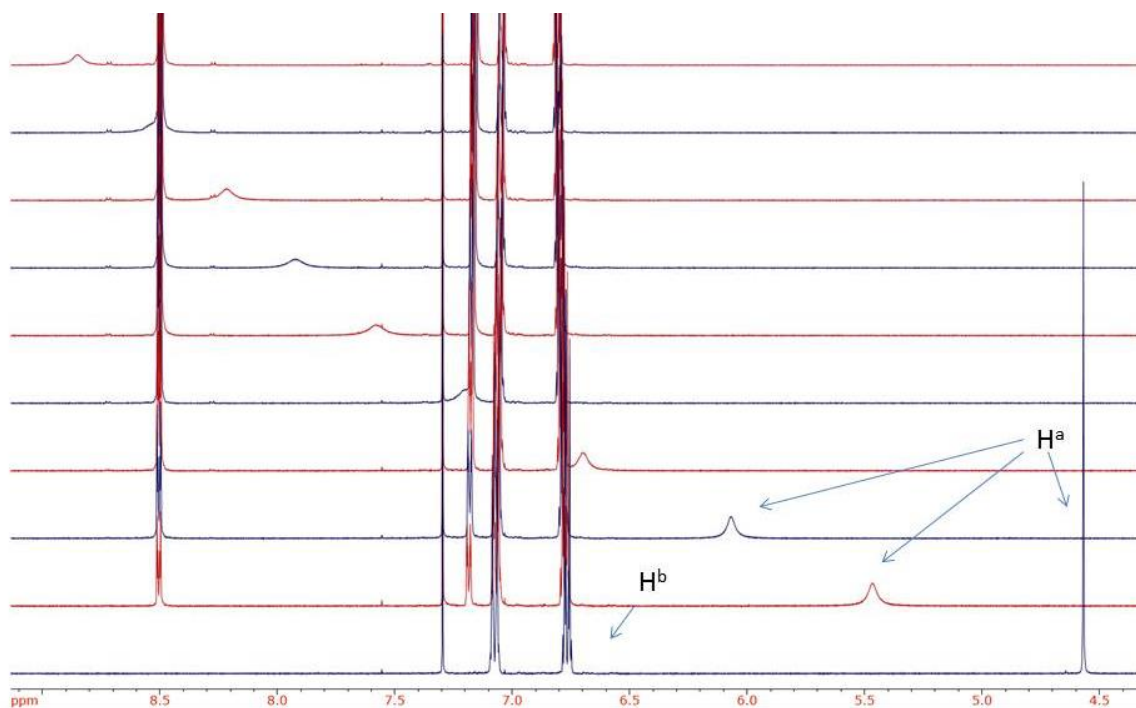


Figure S4.3: partial 400.2 MHz ^1H NMR spectra of titration in chloroform with monitored signals labelled.

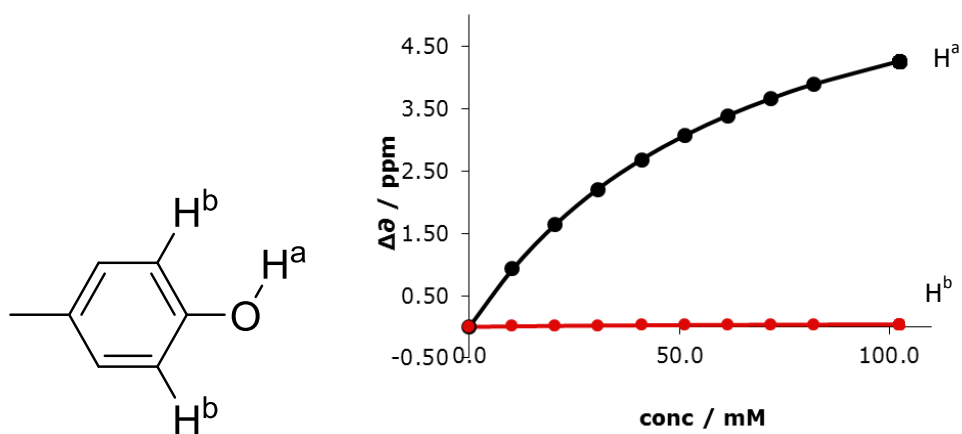


Figure S4.4: Binding isotherm for titration

$$K_a = 19 \pm 2 \text{ M}^{-1} \quad 64\% \text{ bound}$$

Titration of 2-fluoro-4-methylphenol with 4-picoline in toluene

Host: 2-fluoro-4-methylphenol [8 mM]

Guest: 4-picoline

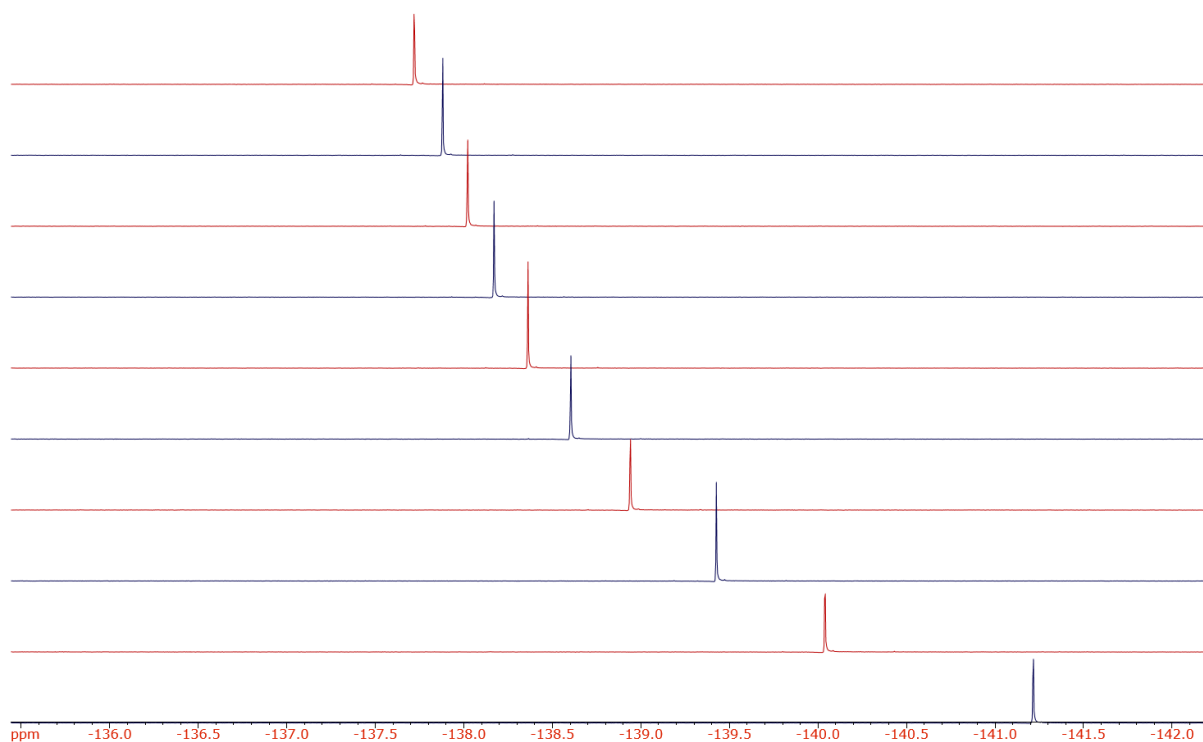


Figure S4.5: partial 376.5 MHz ^{19}F NMR spectra of titration in toluene

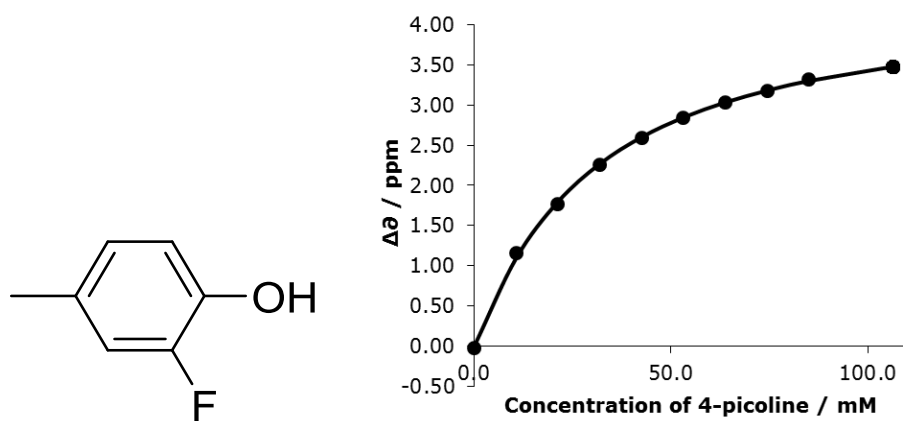


Figure S4.6: Binding isotherm for titration

$$K_a = 40 \pm 1 \text{ M}^{-1} \quad 80\% \text{ bound}$$

Titration of 2-fluoro-4-methylphenol with 4-picoline in chloroform

Host: 2-fluoro-4-methylphenol [14.0 mM]

Guest: 4-picoline

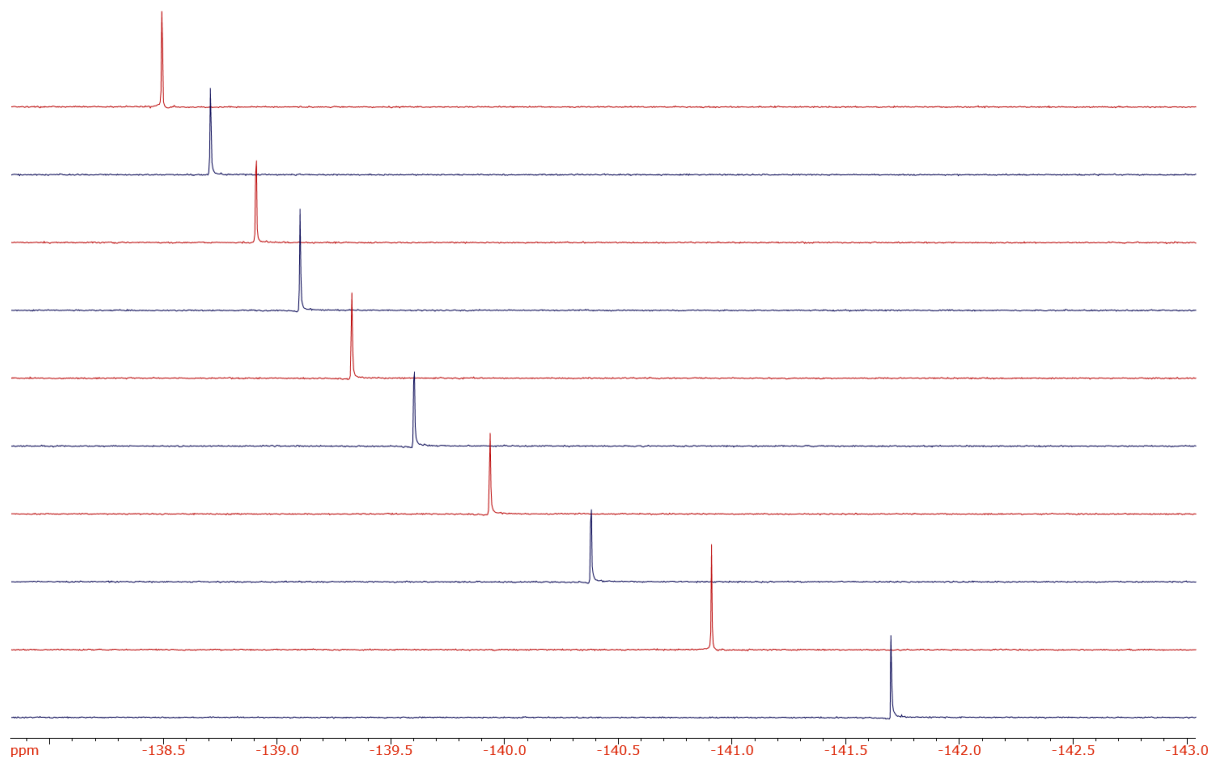


Figure S4.7: partial 376.5 MHz ^{19}F NMR spectra of titration in chloroform

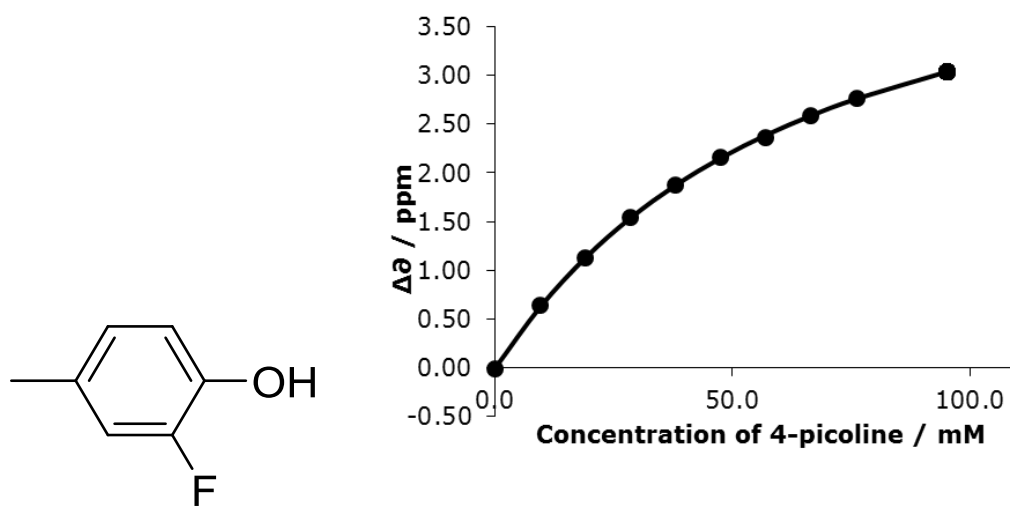


Figure S4.8: Binding isotherm for titration

$$K_a = 20 \pm 1 \text{ M}^{-1} \quad 62\% \text{ bound}$$

Titration of 3-fluoro-4-methylphenol with 4-picoline in toluene

Host: 3-fluoro-4-methylphenol [4.44 mM]

Guest: 4-picoline

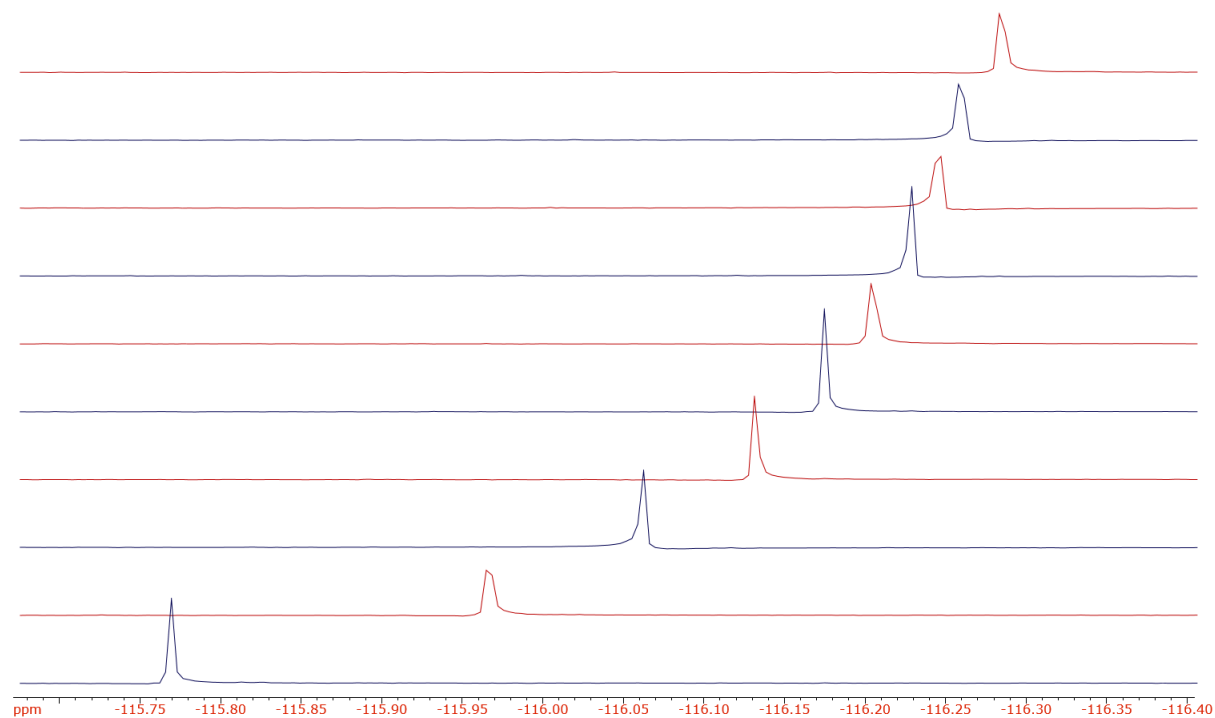


Figure S4.9: partial 376.5 MHz ^{19}F NMR spectra of titration in toluene

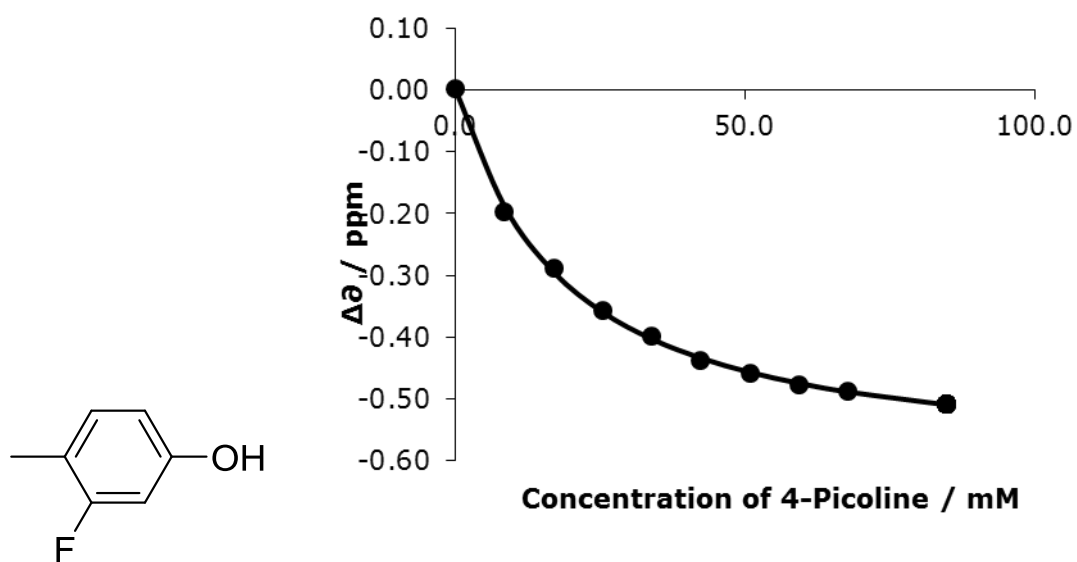


Figure S4.10: Binding isotherm for titration

$$K_a = 62 \pm 5 \text{ M}^{-1} \quad 84\% \text{ bound}$$

Titration of 3-fluoro-4-methylphenol with 4-picoline in chloroform

Host: 3-fluoro-4-methylphenol [14.2 mM]

Guest: 4-picoline



Figure S4.11: partial 376.5 MHz ^{19}F NMR spectra of titration in chloroform

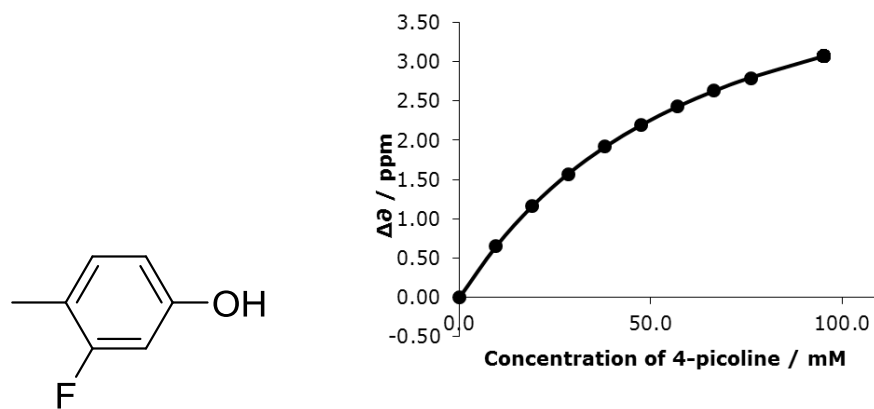


Figure S4.12: Binding isotherm for titration

$$K_a = 52 \pm 1 \text{ M}^{-1} \quad 78\% \text{ bound}$$

Titration of pentafluorophenol with 4-picoline in toluene

Host: pentafluorophenol [4 mM]

Guest: 4-picoline

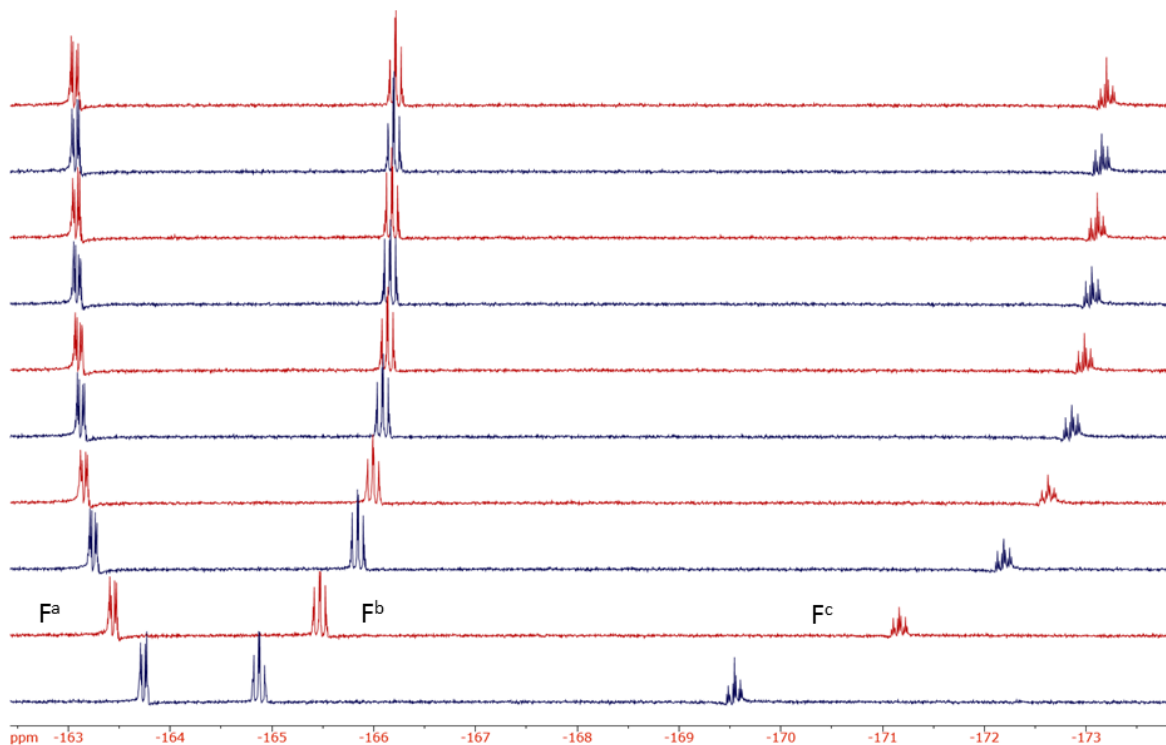


Figure S4.13: partial 376.5 MHz ^{19}F NMR spectra of titration in toluene

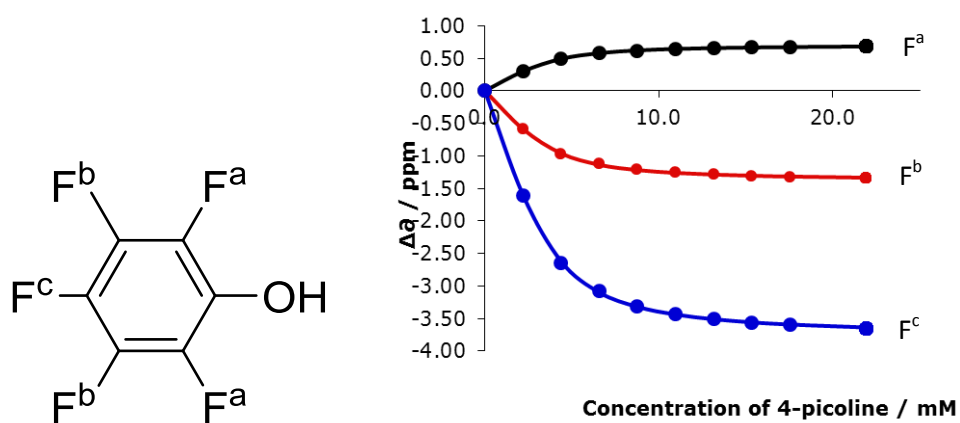


Figure S4.14: Binding isotherms for titration

$$K_a = 1300 \pm 50 \text{ M}^{-1} \quad 96\% \text{ bound}$$

Titration of pentafluorophenol with 4-picoline in chloroform

Host: pentafluorophenol [2 mM]

Guest: 4-picoline

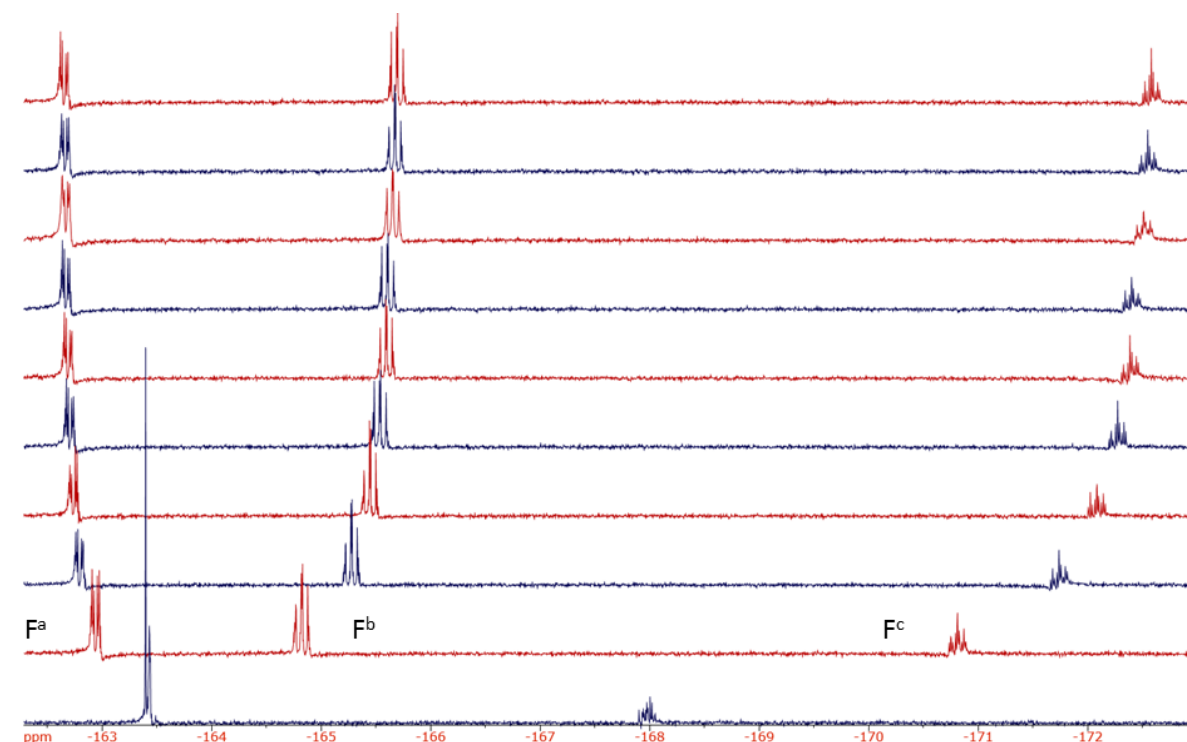


Figure S4.15: partial 376.5 MHz ^{19}F NMR spectra of titration in chloroform

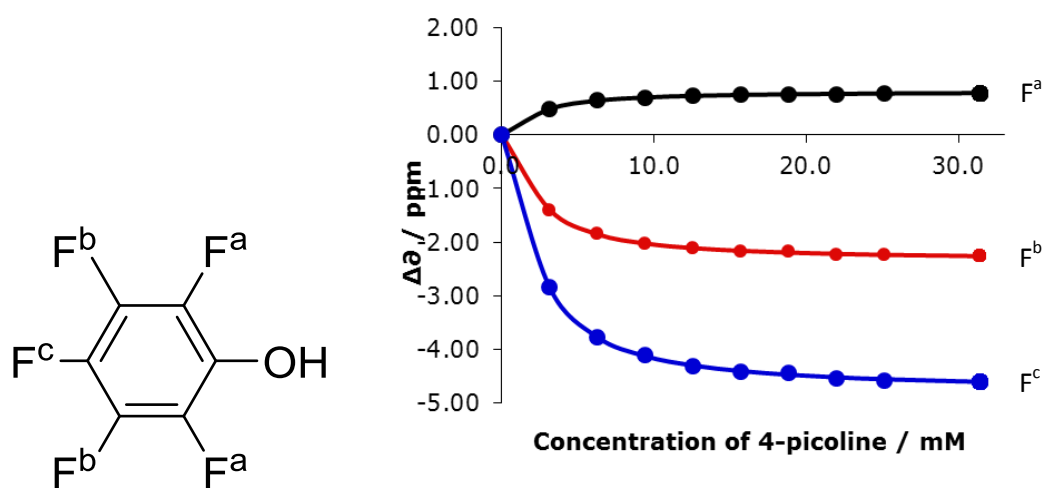


Figure S4.16: Binding isotherms for titration

$$K_a = 850 \pm 60 \text{ M}^{-1} \quad 96\% \text{ bound}$$

Titration of pentafluorophenol with 4-picoline in acetonitrile

Host: pentafluorophenol [12 mM]

Guest: 4-picoline

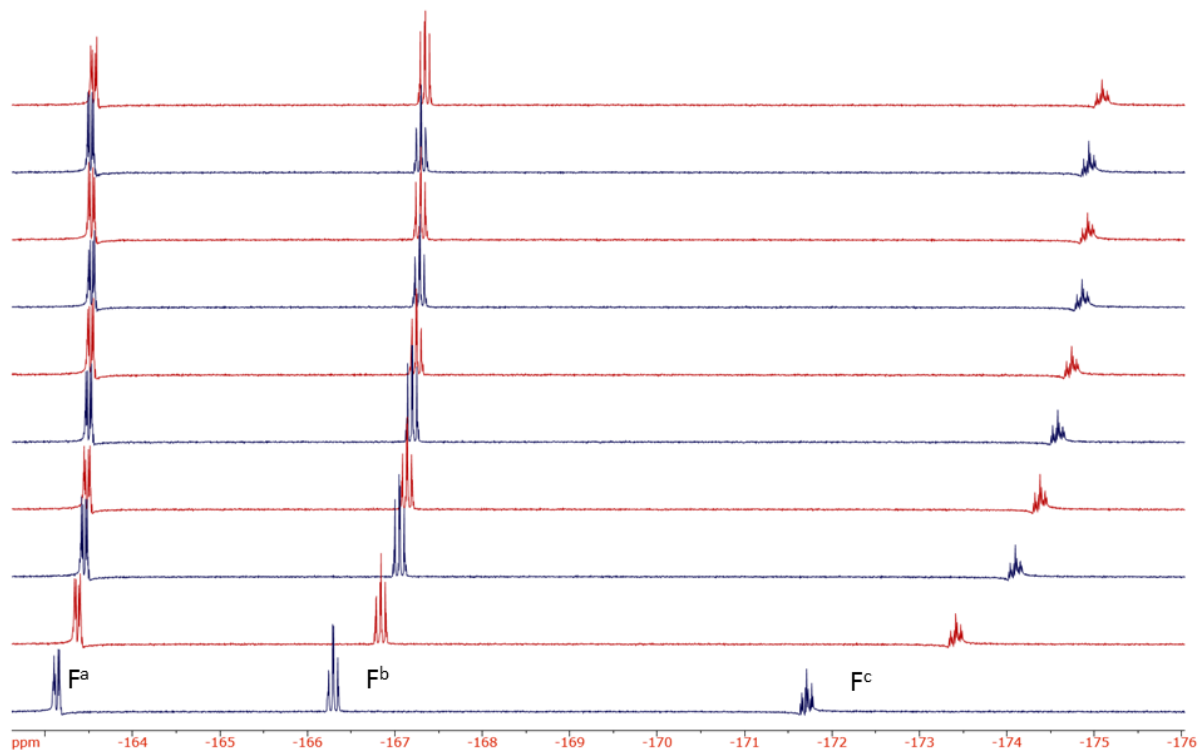


Figure S4.17: partial 376.5 MHz ^{19}F NMR spectra of titration in acetonitrile

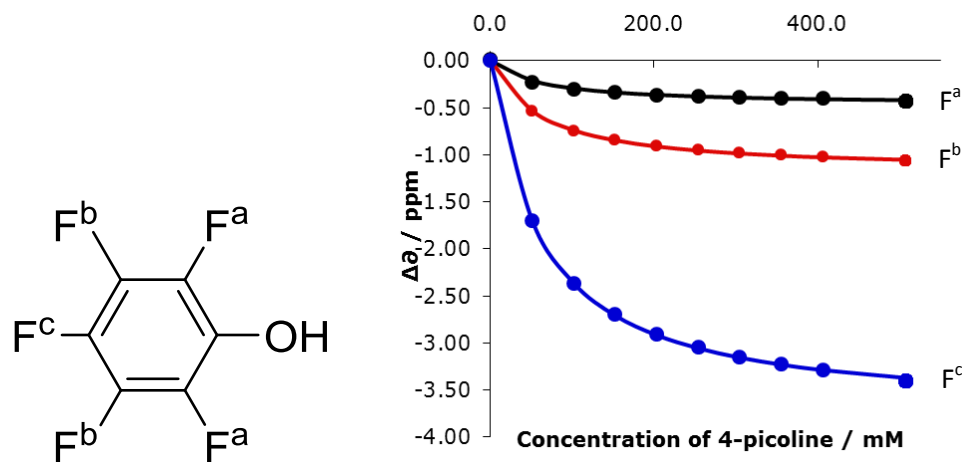


Figure S4.18: Binding isotherms for titration

$$K_a = 19 \pm 1 \text{ M}^{-1} \quad 90\% \text{ bound}$$

Titration of pentafluoriodobenzene with 4-picoline in toluene

Host: pentafluorophenol [100 mM]

Guest: 4-picoline

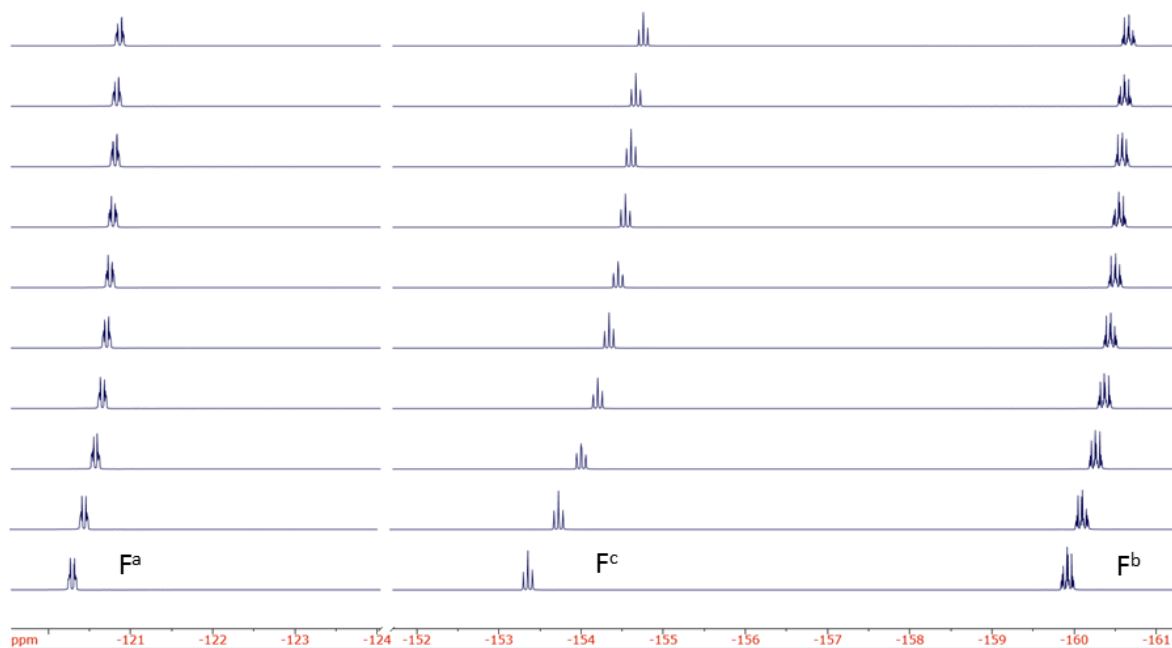


Figure S4.19: partial 376.5 MHz ^{19}F NMR spectra of titration in toluene

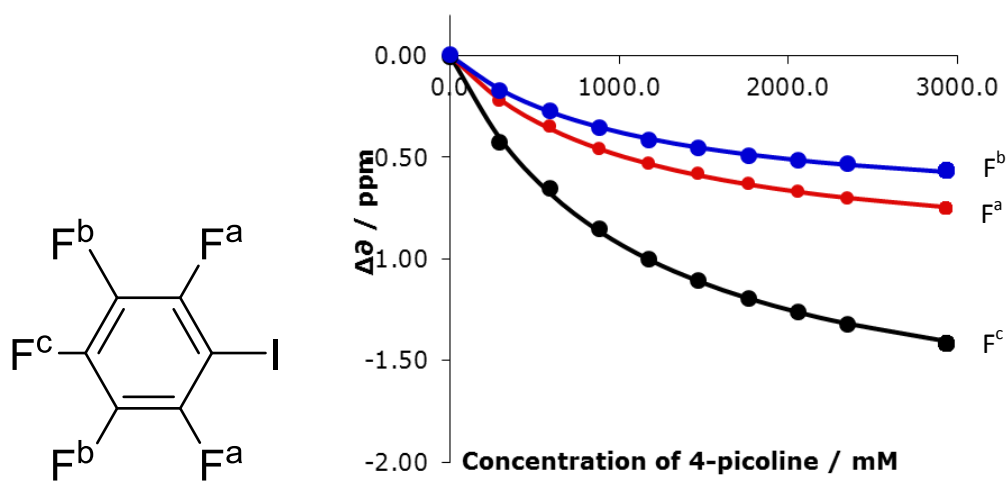
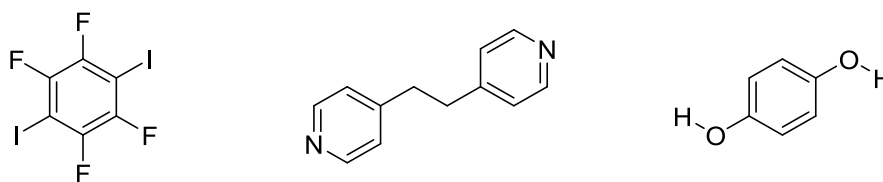


Figure S4.20: Binding isotherm for titration

$$K_a = 1 \pm 1 \text{ M}^{-1} \quad 74\% \text{ bound}$$

5. Synthesis of Co-Crystals

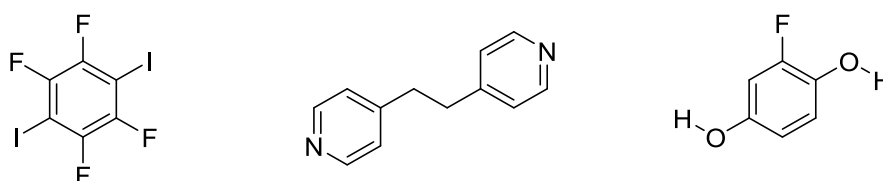
System A



An equimolar quantity of hydroquinone (0.044 g, 0.40 mmol, 1 eq.), 1,4-diiidotetrafluorobenzene (0.16 g, 0.40 mmol, 1 eq.) and 1,2-bis(4-pyridyl)ethane (0.074 g, 0.40 mmol, 1 eq.) were dissolved in the appropriate solvent (100 mL, co-crystallisation concentration 4.0 mM) and the solution placed on a polystyrene box lid to minimise vibrations and the solvent was allowed to slowly evaporate at ambient temperature. The co-crystals which formed after 24 h were isolated by filtration, dried and then investigated by powder X-ray diffraction. The yields of co-crystals, according to their subsequent identity from X-ray powder diffraction, from each solvent were as follows:

Toluene (0.08 g, 68% HB), Chloroform (0.134 g, 20% HB & 47% XB), Dichloromethane (0.086 g, 66% HB & 3% XB), Acetone (0.21 g, 90% XB), Acetonitrile (0.19 g, 81% XB), Nitromethane (0.17 g, 73% XB), Propan-2-ol (0.12 g, 51% XB).

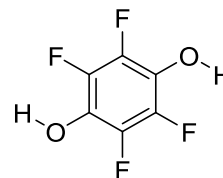
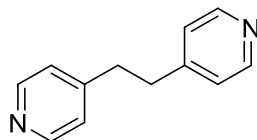
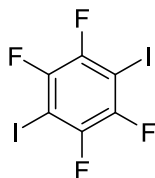
System B



An equimolar quantity of fluorohydroquinone (0.064 g, 0.50 mmol, 1 eq.), 1,4-diiidotetrafluorobenzene (0.20 g, 0.50 mmol, 1 eq.) and 1,2-bis(4-pyridyl)ethane (0.092 g, 0.50 mmol, 1 eq.) were dissolved in the appropriate solvent (125 mL, co-crystallisation concentration 4.0 mM) and the solution placed on a polystyrene box lid to minimise vibrations and the solvent was allowed to slowly evaporate at ambient temperature. The co-crystals which formed after 24 h were isolated by filtration, dried and then investigated by powder X-ray diffraction. The yields of co-crystals from each solvent were as follows:

Toluene (0.115 g, 74% HB), Chloroform (0.105 g, 67% HB), Dichloromethane (0.105 g, 61% HB & 3% XB), Acetone (0.19 g, 65% XB), Acetonitrile (0.135 g, 46% XB), Nitromethane (0.20 g, 68% XB), Propan-2-ol (0.19 g, 65% XB).

System C



An equimolar quantity of tetrafluorohydroquinone (0.1 g, 0.55 mmol, 1 eq.), 1,4-diodotetrafluorobenzene (0.22 g, 0.55 mmol, 1 eq.) and 1,2-bis(4-pyridyl)ethane (0.1 g, 0.55 mmol, 1 eq.) were dissolved in the appropriate solvent (100 mL, co-crystallisation concentration 5.5 mM) and the solution placed on a polystyrene box lid to minimise vibrations. The solvent was allowed to slowly evaporate at ambient temperature and co-crystals which formed after 24 h were isolated by filtration, dried and then investigated by powder X-ray diffraction. The yields of co-crystals from each solvent were as follows:

Toluene (0.17 g, 85% HB), Chloroform (0.125 g, 62% HB), Dichloromethane (0.105 g, 52% HB), Acetone (0.115 g, 57% HB), Acetonitrile (0.1 g, 50% HB), Nitromethane (0.09 g, 45% HB), Propan-2-ol (0.20 g, 58% HB & 26% XB).

6. Full Table of Powder X-Ray Diffraction Results

Table S2. Table of co-crystal compositions for systems **A**, **B** and **C** obtained from the seven solvents.

| | System A | System B | System C |
|---------------------------------|------------------|-----------------|------------------|
| Toluene | 100% HB | 100% HB | 100% HB |
| CHCl ₃ | 30% HB 70% XB | 100% HB | 100% HB |
| CH ₂ Cl ₂ | 95% HB 5% XB | 95% HB 5% XB | 100% HB |
| Acetone | 100% XB | 100% XB | 100% HB |
| MeCN | 100% XB | 100% XB | 100% HB |
| NO ₂ Me | 100% XB | 100% XB | 100% HB |
| <i>i</i> -Propanol | 100% XB | 100% XB | 69% HB 31% XB |

7. Phase Purity Analysis by XRPD: Experimental Description

Microcrystalline powder samples for analysis by XRPD were loaded into 0.7 mm borosilicate capillaries. X-ray diffraction data were collected using either synchrotron radiation at beamline I11 at Diamond Light Source^{S1,S2} or at the University of Sheffield using a Bruker D8 ADVANCE X-ray powder diffractometer.

Synchrotron data were collected at different wavelengths (all close to 0.82 Å; specific values reported for each experiment) and the instrument was equipped with a wide angle (90°) PSD detector comprising 18 Mythen-2 modules. A pair of scans was conducted at room temperature, related by a 0.25° detector offset to account for gaps between detector modules. Five such scan pairs were collected at 10 s exposure, preceded and followed by a pair of 1 s scans to compare to check for beam damage. The resulting patterns were summed to give the final pattern for structural analysis (total beam exposure time therefore 104 s).

In house X-ray diffraction data was collected a Cu K α Bruker D8 ADVANCE X-Ray powder diffractometer. The instrument was fitted with a focusing Göbel mirror optic and a high resolution energy-dispersive Lynxeye XE detector. Scans were collected at room temperature between 5-60° 2 θ , using a step size of 0.01532° and step time of 14 s giving a total exposure time of 15 h.

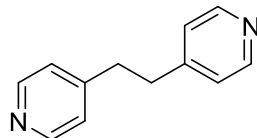
Powder pattern indexing and fitting was carried out using the TOPAS program.^{S3}

When fitting powder patterns collected for the starting materials, pure HB or XB networks or from competition experiments in Systems **A-C**, the patterns were compared with calculated X-ray powder patterns established from single-crystal X-ray diffraction. The unit cell parameters from the pure HB or XB phases were used as a starting point for the Pawley fitting^{S5} of the competition experiment results. Fitting was conducted over a selected 2 θ range, based on the visible presence of peaks in each pattern. The fit range is described beneath each figure. For mixed-phase patterns, Rietveld fitting^{S10} was employed to establish the relative quantities of each phase.

8. Phase Purity Checks by XRPD: Compounds 1,2a, 2b, 2c and 3

The phase purity of the as-purchased materials used in the crystal syntheses were checked by X-ray powder diffraction before use.

Phase-purity check, 1,2-bis(4-pyridyl)ethane (**3**)

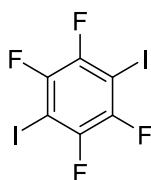


X-ray diffraction data of the white crystalline powder were collected using synchrotron radiation ($\lambda = 0.82562(1) \text{ \AA}$). The pattern was compared with calculated X-ray powder patterns for **3** already established from single-crystal X-ray diffraction (CSD refcode ZEXKIW).^{S4} The unit cell parameters of **3** were used as a starting point for Pawley refinement,^{S5} employing 704 parameters (8 background, 1 zero error, 5 profile, 4 cell, 686 reflections). Pawley refinement converged to $R_{wp} = 0.0517$, $R_{wp}' = 0.1304$. [$a = 5.55908(3) \text{ \AA}$, $b = 8.16704(3) \text{ \AA}$, $c = 11.36448(8) \text{ \AA}$, $\beta = 100.6657(6)^\circ$, $V = 507.048(5) \text{ \AA}^3$].



Figure S8.1. Observed (blue) and calculated (red) profiles and difference plot [$I_{obs} - I_{calc}$] (grey) of the Pawley refinement. (2θ range $6.8 - 53^\circ$, $d_{min} = 0.92 \text{ \AA}$).

Phase-purity check, perfluoro-1,4-diiodobenzene (**1**)



X-ray diffraction data of the white microcrystalline powder was collected using Cu K α radiation. The pattern was compared with calculated X-ray powder patterns for **1** already established from single-crystal X-ray diffraction (CSD refcode ZZZAVM).^{S6} The unit cell parameters of **1** were used as a starting point for Pawley refinement,^{S5} employing 147 parameters (8 background, 1 zero error, 5 profile, 4 cell, 125 reflections). Pawley refinement converged to $R_{wp} = 0.0294$, $R_{wp}' = 0.0942$. [$a = 6.2529$ (1) Å, $b = 11.6040$ (2) Å, $c = 5.9178$ (1) Å, $\beta = 92.608$ (1) °, $V = 428.94$ (1) Å³].

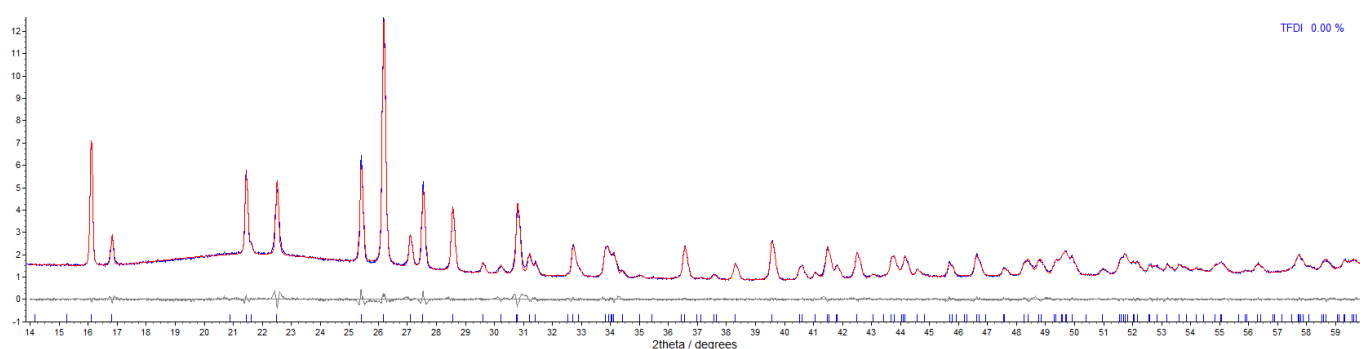
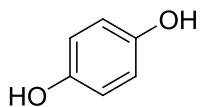


Figure S8.2. Observed (blue) and calculated (red) profiles and difference plot [$I_{\text{obs}} - I_{\text{calc}}$] (grey) of the Pawley refinement. (2θ range 14 - 60 °, $d_{\text{min}} = 1.54$ Å).

Phase-purity check, hydroquinone (**2a**)



X-ray diffraction data of the white microcrystalline powder were collected using synchrotron radiation ($\lambda = 0.82562$ (1) Å). The pattern was compared with calculated X-ray powder patterns for **2a** already established from single-crystal X-ray diffraction (CSD refcode HYQUIN02).^{S7} The unit cell parameters of **2a** were used as a starting point for Pawley refinement,^{S5} employing 1423 parameters (18 background, 1 zero error, 5 profile, 2 cell, 1397 reflections). Pawley refinement converged to $R_{wp} = 0.0142$, $R_{wp}' = 0.0750$ [$a = b = 38.5225(2)$ Å, $c = 5.6594$ (1) Å, $V = 7273.2$ (1) Å³].

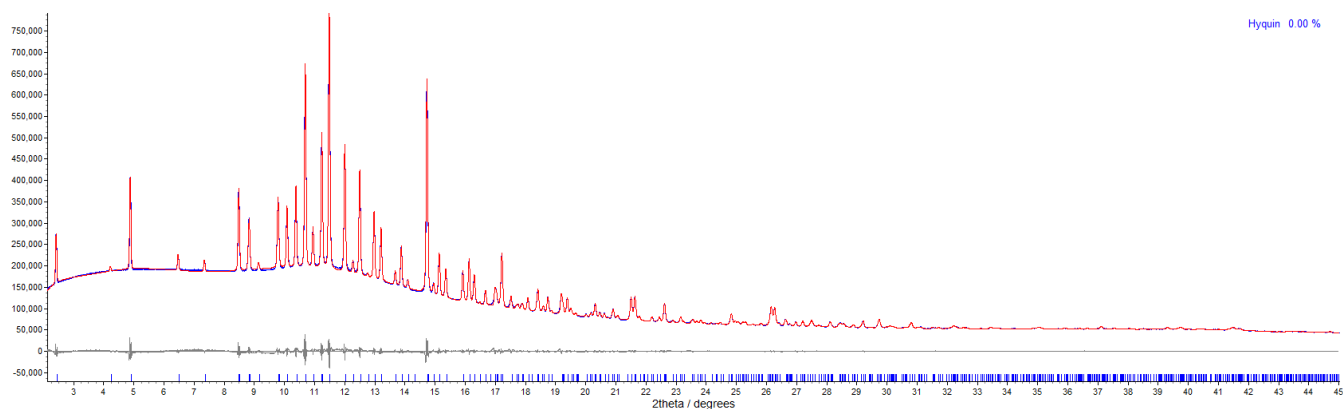
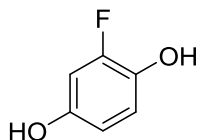


Figure S8.3. Observed (blue) and calculated (red) profiles and difference plot [$I_{\text{obs}} - I_{\text{calc}}$] (grey) of the Pawley refinement. (2θ range 2.0 - 45 °, $d_{\text{min}} = 1.08$ Å).

Phase-purity check, 2-fluorohydroquinone (**2b**)



X-ray diffraction data of the off-white microcrystalline powder were collected using synchrotron radiation ($\lambda = 0.82582(1) \text{ \AA}$). The pattern was compared with calculated X-ray powder patterns for **2b**, which has established from single-crystal X-ray diffraction.^{S8} The unit cell parameters of **2b** were used as a starting point for Pawley refinement,^{S4} employing 1675 parameters (16 background, 1 zero error, 5 profile, 6 cell, 1647 reflections). Pawley refinement converged to $R_{wp} = 0.0161$, $R_{wp}' = 0.0781$. [$a = 5.59470(4) \text{ \AA}$, $b = 9.91526(6) \text{ \AA}$, $c = 14.15526(9) \text{ \AA}$, $\alpha = 109.3048(3)^\circ$, $\beta = 97.5352(3)^\circ$, $\gamma = 100.5002(2)^\circ$, $V = 713.008(8) \text{ \AA}^3$].

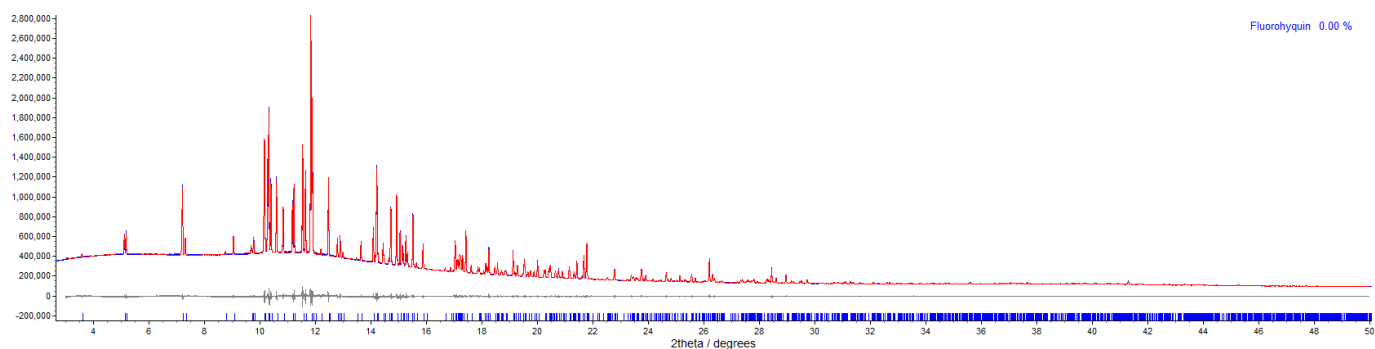
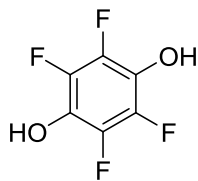


Figure S8.4. Observed (blue) and calculated (red) profiles and difference plot [$I_{\text{obs}} - I_{\text{calc}}$] (grey) of the Pawley refinement. (2θ range 3 – 50 $^\circ$, $d_{\text{min}} = 0.98 \text{ \AA}$).

Phase-purity check, perfluorohydroquinone (**2c**)



X-ray diffraction data of the off-white microcrystalline powder were collected using synchrotron radiation ($\lambda = 0.82582(1) \text{ \AA}$). The pattern was compared with calculated X-ray powder patterns for **2c** already established from single-crystal X-ray diffraction (CSD refcode GUFMAV).^{S9} The unit cell parameters of **2c** were used as a starting point for Pawley refinement,^{S4} employing 599 parameters (6 background, 1 zero error, 5 profile, 4 cell, 583 reflections). Pawley refinement converged to $R_{wp} = 0.0613$, $R_{wp}' = 0.1491$. [$a = 6.55976(4) \text{ \AA}$, $b = 4.88392(3) \text{ \AA}$, $c = 10.25333(6) \text{ \AA}$, $\beta = 109.4872(5)^\circ$, $V = 309.672(3) \text{ \AA}^3$].

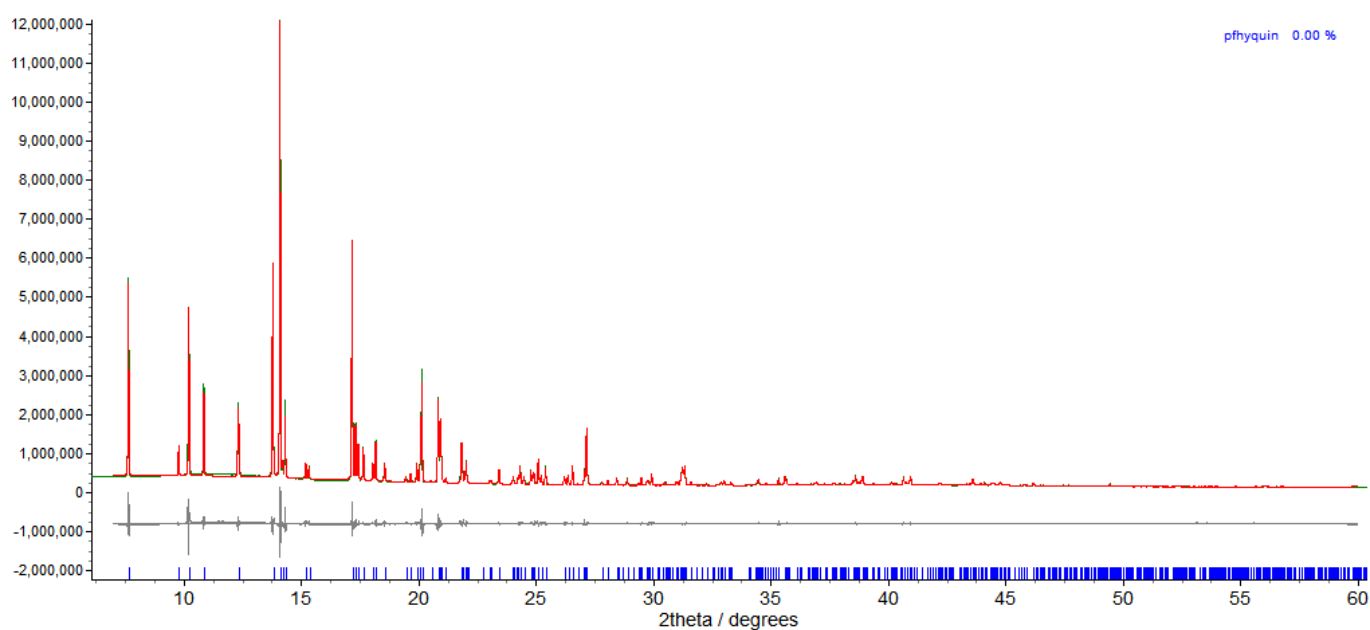
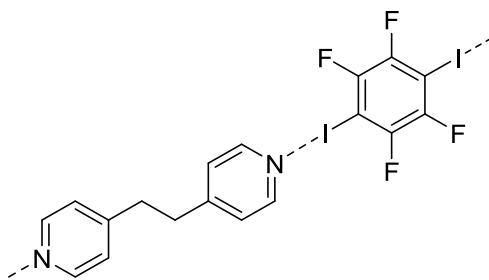


Figure S8.5. Observed (green) and calculated (red) profiles and difference plot [$I_{obs} - I_{calc}$] (grey) of the Pawley refinement. (2θ range 7.0 – 60 °, $d_{min} = 0.83 \text{ \AA}$).

9. Phase Purity Check by XRPD: Co-crystals **1•3**, **2a•3**, **2b•3** and **2c•3**

The X-ray powder diffraction patterns of the microcrystalline products resulting from mixing of only two of the components from each set of competition experiments was recorded. This was to investigate and determine experimentally the formation of the hydrogen-bonding only and halogen-bonding only phases, in the absence of a competing reagent.

Two-component co-crystallisation (System A-C, **1 + 3**)



X-ray diffraction data of the white microcrystalline powder were collected using synchrotron radiation ($\lambda = 0.82652 (1) \text{ \AA}$). The pattern was compared with calculated X-ray powder patterns for **1•3** (the halogen-bonded co-crystal phase) already established from single-crystal X-ray diffraction (crystal structure taken from CSD refcode MEKWO0).^{S10} The unit cell parameters of **1•3** were used as a starting point for Pawley refinement,^{S5} employing 1114 parameters (6 background, 1 zero error, 5 profile, 6 cell, 1096 reflections). Pawley refinement converged to $R_{wp} = 0.0587$, $R_{wp}' = 0.1454$. [$a = 5.04863 (3) \text{ \AA}$, $b = 9.92166 (7) \text{ \AA}$, $c = 10.6267 (1) \text{ \AA}$, $\alpha = 64.7567 (7)^\circ$, $\beta = 82.0664 (7)^\circ$, $\gamma = 87.8850 (4)^\circ$, $V = 476.717 (7) \text{ \AA}^3$].

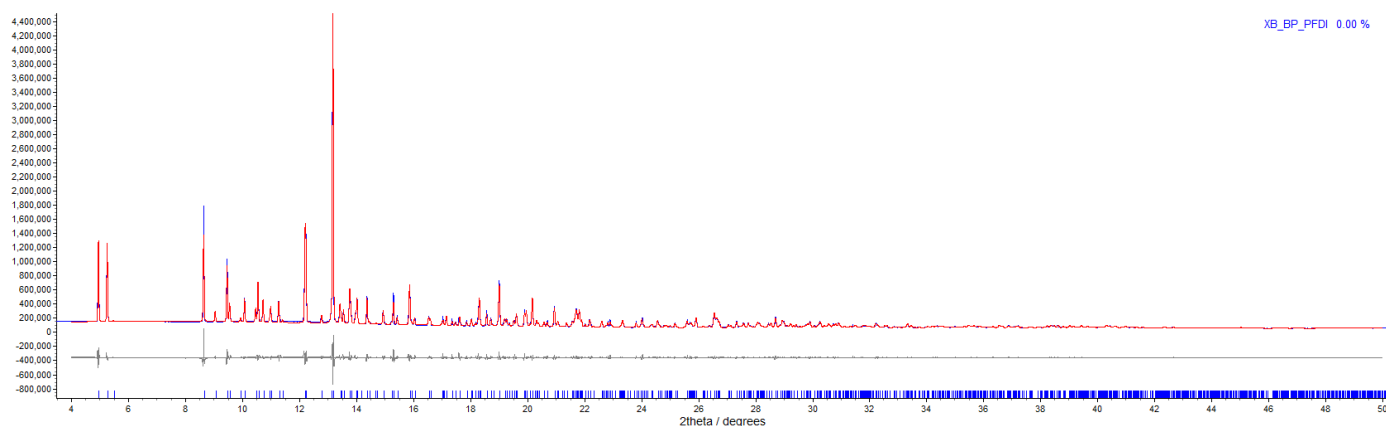
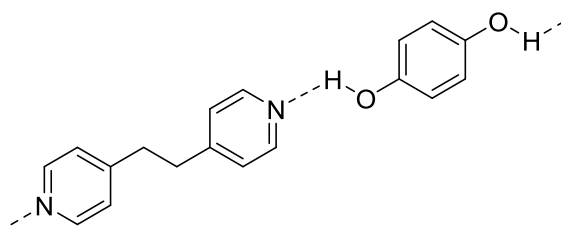


Figure S9.1. Observed (blue) and calculated (red) profiles and difference plot [$I_{\text{obs}} - I_{\text{calc}}$] (grey) of the Pawley refinement. (2θ range $5.0 - 50^\circ$, $d_{\text{min}} = 0.97 \text{ \AA}$).

Two-component co-crystallisation (System A, 2a + 3)



X-ray diffraction data of the white microcrystalline powder were collected using synchrotron radiation ($\lambda = 0.82652(1) \text{ \AA}$). The pattern was compared with calculated X-ray powder patterns for **2a•3** (the hydrogen-bonded co-crystal phase) already established from single-crystal X-ray diffraction.^{S10} The unit cell parameters of **2a•3** were used as a starting point for Pawley refinement,^{S5} employing 1641 parameters (8 background, 1 zero error, 5 profile, 6 cell, 1621 reflections). Pawley refinement converged to $R_{wp} = 0.0499$, $R_{wp}' = 0.0636$. [$a = 7.43927(5) \text{ \AA}$, $b = 9.43980(5) \text{ \AA}$, $c = 11.8509(1) \text{ \AA}$, $\alpha = 95.2651(6)^\circ$, $\beta = 92.9887(7)^\circ$, $\gamma = 108.1735(6)^\circ$, $V = 784.51(1) \text{ \AA}^3$].

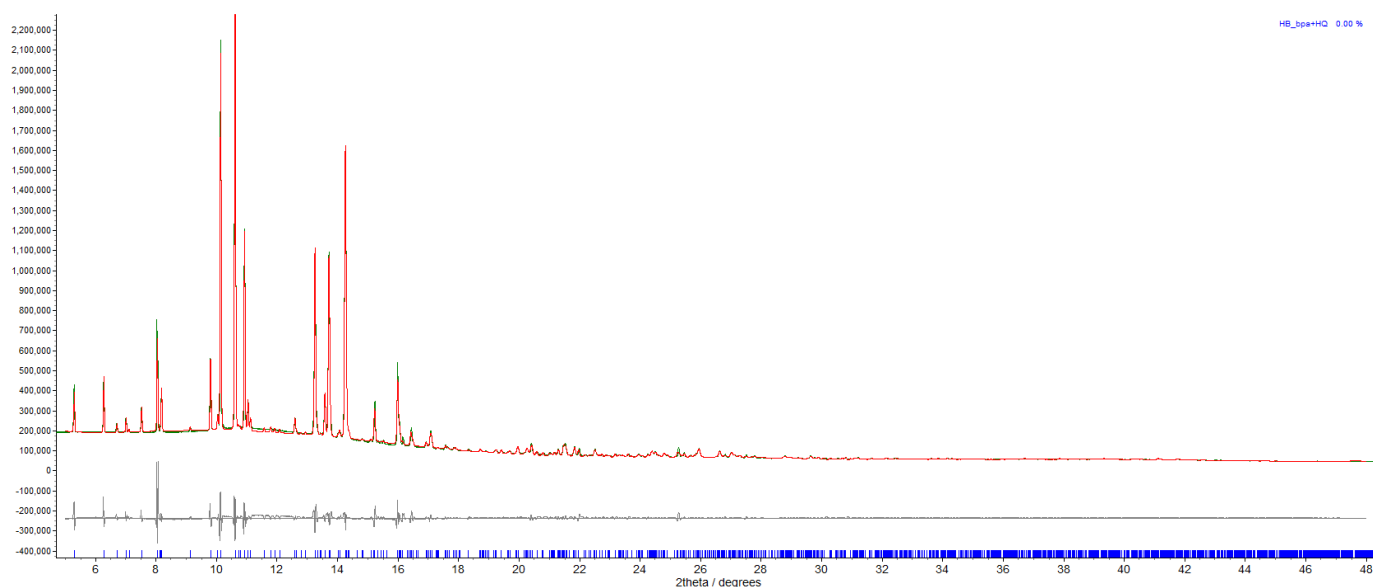
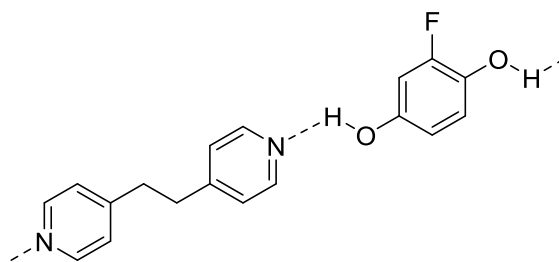


Figure S9.2. Observed (green) and calculated (red) profiles and difference plot $[I_{obs} - I_{calc}]$ (grey) of the Pawley refinement. (2θ range $5.0 - 48^\circ$, $d_{min} = 1.02 \text{ \AA}$).

Two-component co-crystallisation (System B, 2b + 3)



X-ray diffraction data of the white microcrystalline powder was collected in house. The pattern was compared with calculated X-ray powder patterns for **2b•3** (the hydrogen-bonded co-crystal phase), which has been established from single-crystal X-ray diffraction and is reported herein. The unit cell parameters of **2b•3** were used as a starting point for Pawley refinement,^{S5} employing 444 parameters (12 background, 1 zero error, 5 profile, 6 cell, 420 reflections). Pawley refinement converged to $R_{wp} = 0.0199$, $R_{wp}' = 0.0498$. [$a = 7.4266$ (1) Å, $b = 9.4109$ (1) Å, $c = 11.9305$ (2) Å, $\alpha = 96.031$ (1) °, $\beta = 92.475$ (1) °, $\gamma = 108.2621$ (6) °, $V = 784.89$ (2) Å³].

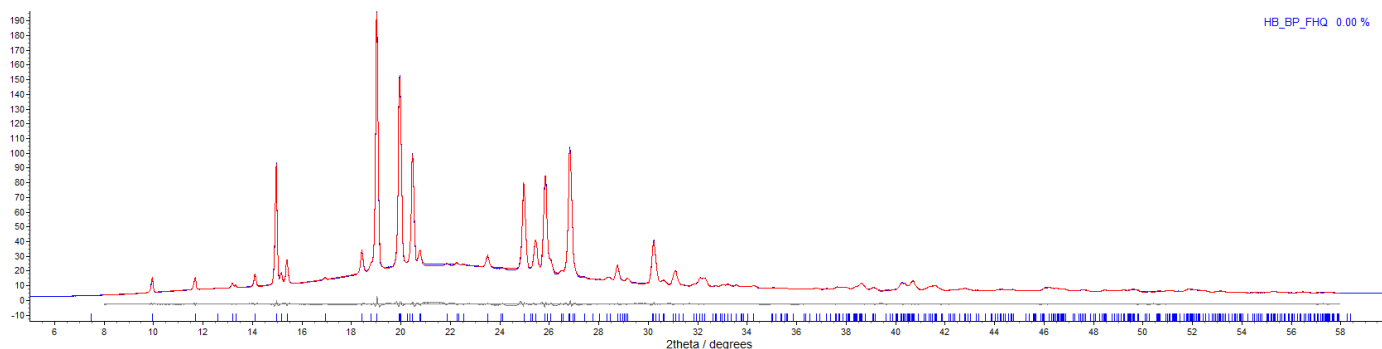
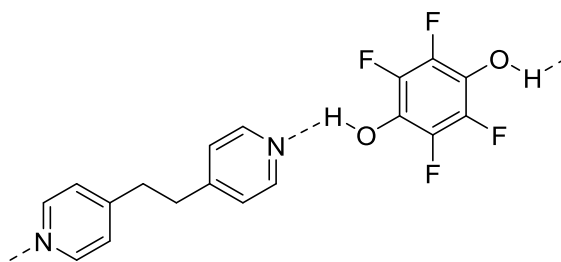


Figure S9.3. Observed (blue) and calculated (red) profiles and difference plot [$I_{\text{obs}} - I_{\text{calc}}$] (grey) of the Pawley refinement. (2θ range 8.0 - 58 °, $d_{\text{min}} = 1.59$ Å).

Two-component co-crystallisation (System C, 2c + 3)



X-ray diffraction data of the white microcrystalline powder was collected using Cu K α radiation. The pattern was compared with calculated X-ray powder patterns for **2c•3** (the hydrogen-bonded co-crystal phase), which has been established from single-crystal X-ray diffraction and is reported herein. The unit cell parameters of **2c•3** were used as a starting point for Pawley refinement,^{S5} employing 249 parameters (14 background, 1 zero error, 5 profile, 6 cell, 223 reflections). Pawley refinement converged to $R_{wp} = 0.0268$, $R_{wp}' = 0.0689$. [$a = 6.3540$ (1) Å, $b = 7.4432$ (1) Å, $c = 9.2267$ (2) Å, $\alpha = 86.134$ (2)°, $\beta = 75.989$ (2)°, $\gamma = 71.302$ (2)°, $V = 401.01$ (2) Å³].

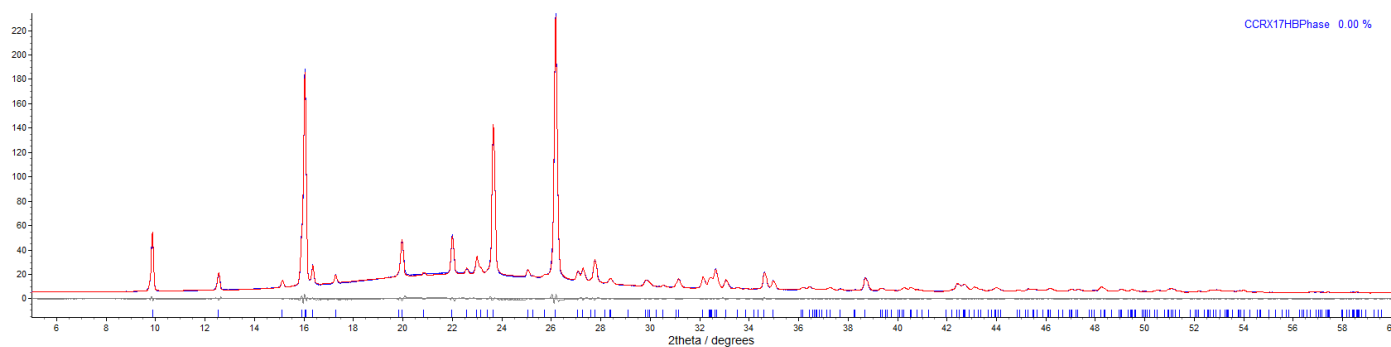
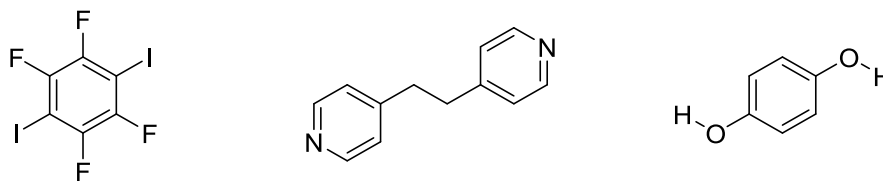


Figure S9.4. Observed (blue) and calculated (red) profiles and difference plot [$I_{\text{obs}} - I_{\text{calc}}$] (grey) of the Pawley refinement. (2θ range 5 - 60°, $d_{\text{min}} = 1.54$ Å).

10. Determination of Product Composition by XRPD: System A

[perfluoro-1,4-diiodobenzene (**1**), hydroquinone (**2a**) and 1,2-bis(4-pyridyl)ethane (**3**)]



The X-ray powder diffraction patterns of the microcrystalline products from all competition experiments were recorded. These were compared to the calculated X-ray powder diffraction patterns for the hydrogen-bonded (**2a•3**) and halogen-bonded (**1•3**) co-crystals as well as the individual components (**1**, **2a** and **3**), before conducting quantitative fitting of the data.

System A: Competition experiment in Toluene.

X-ray diffraction data of the white microcrystalline powder were collected using synchrotron radiation ($\lambda = 0.82582(1) \text{ \AA}$). The pattern was compared with calculated X-ray powder patterns for **2a•3** (the hydrogen-bonded co-crystal phase) for which the crystal structure was already established from single-crystal X-ray diffraction. The unit cell parameters of **2a•3** were used as a starting point for Pawley refinement,^{S5} employing 1637 parameters (11 background, 1 zero error, 5 profile, 6 cell, 1614 reflections). Pawley refinement converged to $R_{wp} = 0.0277$, $R_{wp}' = 0.0918$. [$a = 7.42363(5) \text{ \AA}$, $b = 9.42107(6) \text{ \AA}$, $c = 11.81438(9) \text{ \AA}$, $\alpha = 95.345(1)^\circ$, $\beta = 92.998(1)^\circ$, $\gamma = 108.1405(6)^\circ$, $V = 778.91(1) \text{ \AA}^3$].

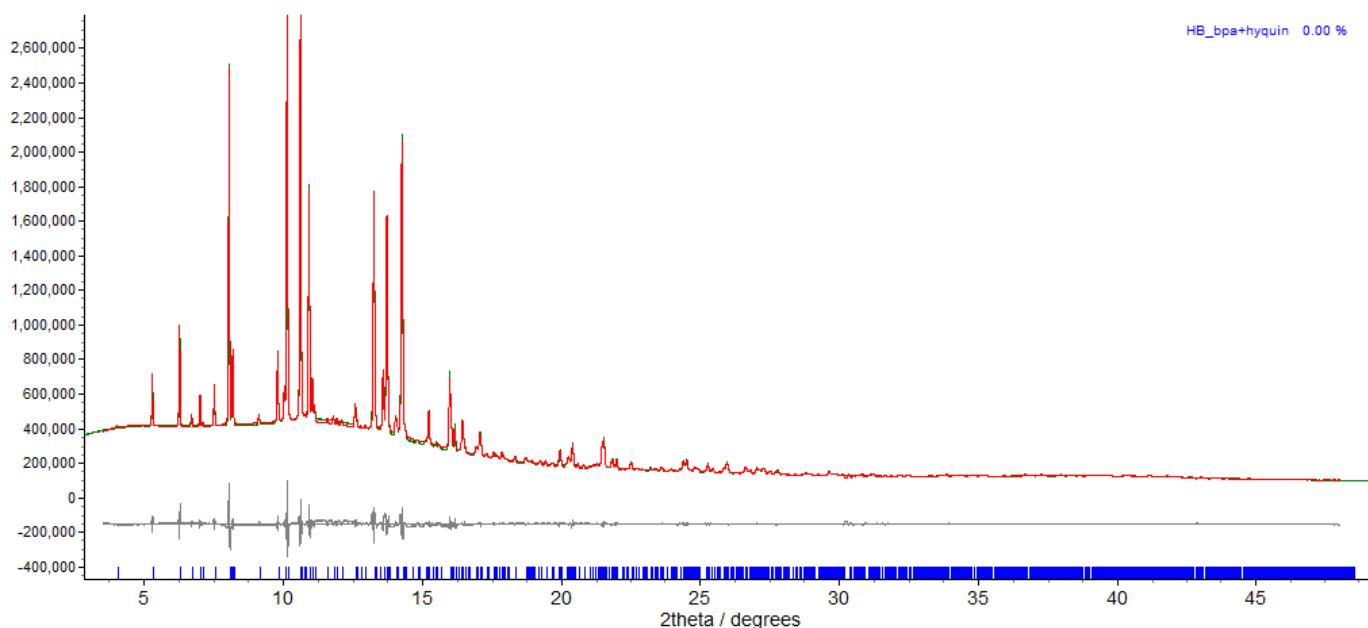


Figure S10.1. Observed (green) and calculated (red) profiles and difference plot [$I_{\text{obs}}-I_{\text{calc}}$] (grey) of the Pawley refinement. (2θ range $3.5 - 48^\circ$, $d_{\text{min}} = 1.01 \text{ \AA}$).

System A: Competition experiment in chloroform.

X-ray diffraction data of the white microcrystalline powder were collected using Cu $K\alpha$ radiation. The pattern was compared with calculated X-ray powder patterns for **2a•3** (the hydrogen-bonded co-crystal phase) and for **1•3** (the halogen-bonded co-crystal phase), for which the crystal structures were already established from single-crystal X-ray diffraction (the halogen-bonded co-crystal phase crystal structure has CSD refcode MEKW00).^{S10} The unit cell parameters of **2a•3** and **1•3** were used as a starting point for a mixed-phase Pawley refinement,^{S5} employing 687 parameters (10 background, 1 zero error, 10 profile, 12 cell, 654 reflections), resulting in final indices of fit $R_{\text{wp}} = 0.0444$, $R_{\text{wp}}' = 0.1088$. The starting model used for the mixed-phase Rietveld refinement,^{S11} conducted using TOPAS, was derived from the single-crystal structures of **2a•3** and **1•3**. A fourth-order spherical harmonics correction term was applied to account for preferred orientation. Refinement employed 51 parameters (11 background, 1 zero error, 10 profile, 12 cell, 2 scale and 15 spherical harmonic terms). Rietveld refinement converged to $R_{\text{wp}} = 0.0733$, $R_{\text{wp}}' = 0.2419$. The relative phase amounts were found to be 30.1 (9) % of **2a•3** and 69.9 (9) % of **1•3**. [**2a•3**: $a = 7.419 (3) \text{ \AA}$, $b = 9.424 (4) \text{ \AA}$, $c = 11.807 (5) \text{ \AA}$, $\alpha = 95.40 (9)^\circ$, $\beta = 93.0 (1)^\circ$, $\gamma = 108.14 (4)^\circ$, $V = 778.1 (6) \text{ \AA}^3$; **1•3**: $a = 5.0374 (4) \text{ \AA}$, $b = 9.9170 (8) \text{ \AA}$, $c = 10.6145 (7) \text{ \AA}$, $\alpha = 64.745 (4)^\circ$, $\beta = 82.103 (6)^\circ$, $\gamma = 87.910 (5)^\circ$, $V = 474.89 (7) \text{ \AA}^3$].

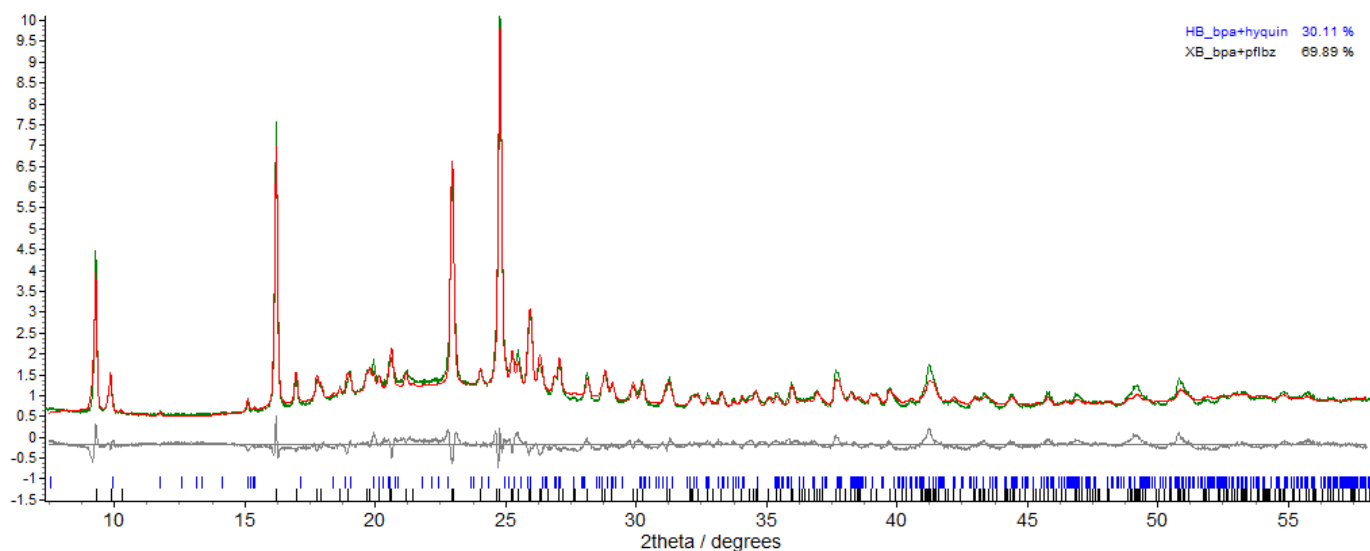


Figure S10.2. Observed (green) and calculated (red) profiles and difference plot [$I_{\text{obs}}-I_{\text{calc}}$] (grey) of the Pawley refinement. (2θ range $7.5 - 58^\circ$, $d_{\text{min}} = 1.59 \text{ \AA}$).

System A: Competition experiment in dichloromethane.

X-ray diffraction data of the white microcrystalline powder were collected using Cu K α radiation. The pattern was compared with calculated X-ray powder patterns for **2a•3** (the hydrogen-bonded co-crystal phase) and for **1•3** (the halogen-bonded co-crystal phase), for which the crystal structures were already established from single-crystal X-ray diffraction (the halogen-bonded co-crystal phase crystal structure has CSD refcode MEKW00).^{S10} The unit cell parameters of **2a•3** and **1•3** were used as a starting point for a mixed-phase Pawley refinement,^{S5} employing 697 parameters (8 background, 1 zero error, 10 profile, 12 cell, 666 reflections), resulting in final indices of fit $R_{wp} = 0.0496$, $R_{wp}' = 0.0822$. The starting model used for the mixed-phase Rietveld refinement,^{S11} conducted using TOPAS, was derived from the single-crystal structures of **2a•3** and **1•3**. Refinement employed 38 parameters (10 background, 1 zero error, 10 profile, 12 cell, 2 scale). Rietveld refinement converged to $R_{wp} = 0.0741$, $R_{wp}' = 0.1407$. The relative phase amounts were found to be 95.05(3) % of **2a•3** and 4.95(3) % of **1•3**. [**2a•3**: $a = 7.4314(2)$ Å, $b = 9.4222(2)$ Å, $c = 11.8156(4)$ Å, $\alpha = 95.333(5)^\circ$, $\beta = 92.993(6)^\circ$, $\gamma = 108.176(2)^\circ$, $V = 779.75(4)$ Å³; **1•3**: $a = 5.0402(5)$ Å, $b = 9.292(1)$ Å, $c = 10.632(9)$ Å, $\alpha = 64.782(6)^\circ$, $\beta = 82.081(8)^\circ$, $\gamma = 87.849(8)^\circ$, $V = 476.30(8)$ Å³].

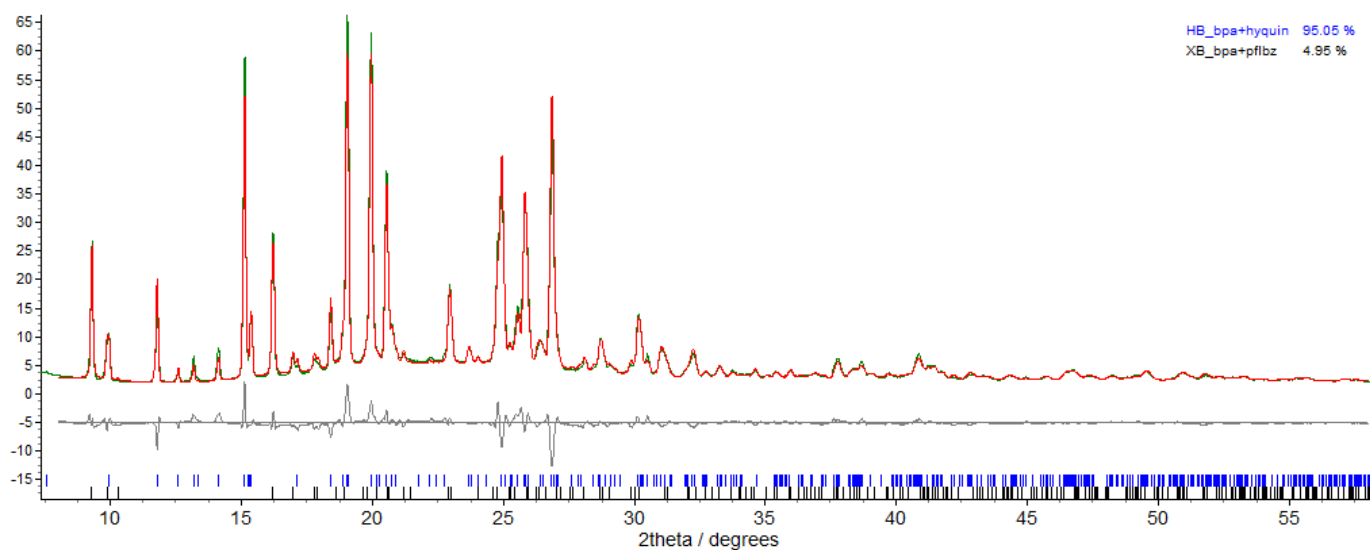


Figure S10.3. Observed (green) and calculated (red) profiles and difference plot [$I_{\text{obs}} - I_{\text{calc}}$] (grey) of the Pawley refinement. (2θ range 8.0 - 58°, $d_{\text{min}} = 1.59$ Å).

System A: Competition experiment in acetone.

X-ray diffraction data of the white microcrystalline powder were collected using synchrotron radiation ($\lambda = 0.82665$ (1) Å). The pattern was compared with calculated X-ray powder pattern for **1•3** (the halogen-bonded co-crystal phase) for which the crystal structure was already established from single-crystal X-ray diffraction (CSD refcode MEKWO0).^{S10} The unit cell parameters of **1•3** were used as a starting point for Pawley refinement,^{S5} employing 880 parameters (6 background, 1 zero error, 5 profile, 6 cell, 862 reflections). Pawley refinement converged to $R_{wp} = 0.0511$, $R_{wp}' = 0.1143$. [$a = 5.04384$ (7) Å, $b = 9.9159$ (1) Å, $c = 10.6266$ (1) Å, $\alpha = 64.7167$ (9) °, $\beta = 82.006$ (1) °, $\gamma = 87.7912$ (9) °, $V = 475.77$ (1) Å³].

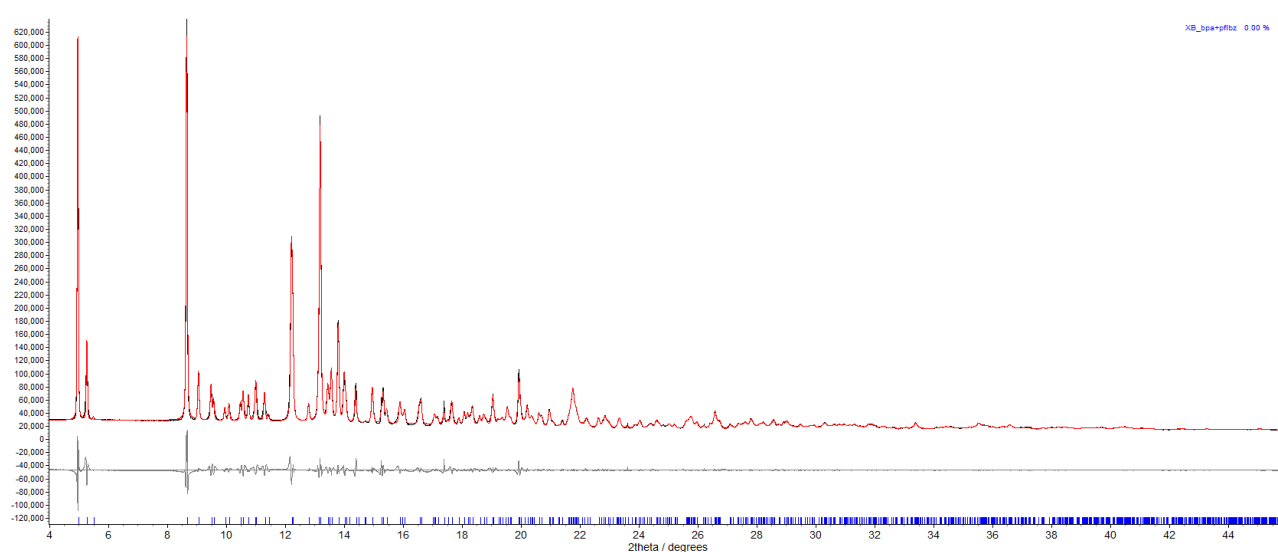


Figure S10.4. Observed (black) and calculated (red) profiles and difference plot [$I_{\text{obs}} - I_{\text{calc}}$] (grey) of the Pawley refinement. (2θ range 4.0 - 46 °, $d_{\text{min}} = 1.06$ Å).

System A: Competition experiment in acetonitrile.

X-ray diffraction data of the white microcrystalline powder were collected using synchrotron radiation ($\lambda = 0.82665(1) \text{ \AA}$). The pattern was compared with calculated X-ray powder pattern for **1•3** (the halogen-bonded co-crystal phase) for which the crystal structure was already established from single-crystal X-ray diffraction (CSD refcode MEKWO0).^{S10} The unit cell parameters of **1•3** were used as a starting point for Pawley refinement,^{S5} employing 604 parameters (6 background, 1 zero error, 5 profile, 6 cell, 586 reflections). Pawley refinement converged to $R_{wp} = 0.0484$, $R_{wp}' = 0.1128$. [$a = 5.04158(7) \text{ \AA}$, $b = 9.9050(2) \text{ \AA}$, $c = 10.6188(1) \text{ \AA}$, $\alpha = 64.789(1)^\circ$, $\beta = 82.155(1)^\circ$, $\gamma = 87.890(1)^\circ$, $V = 475.14(1) \text{ \AA}^3$].

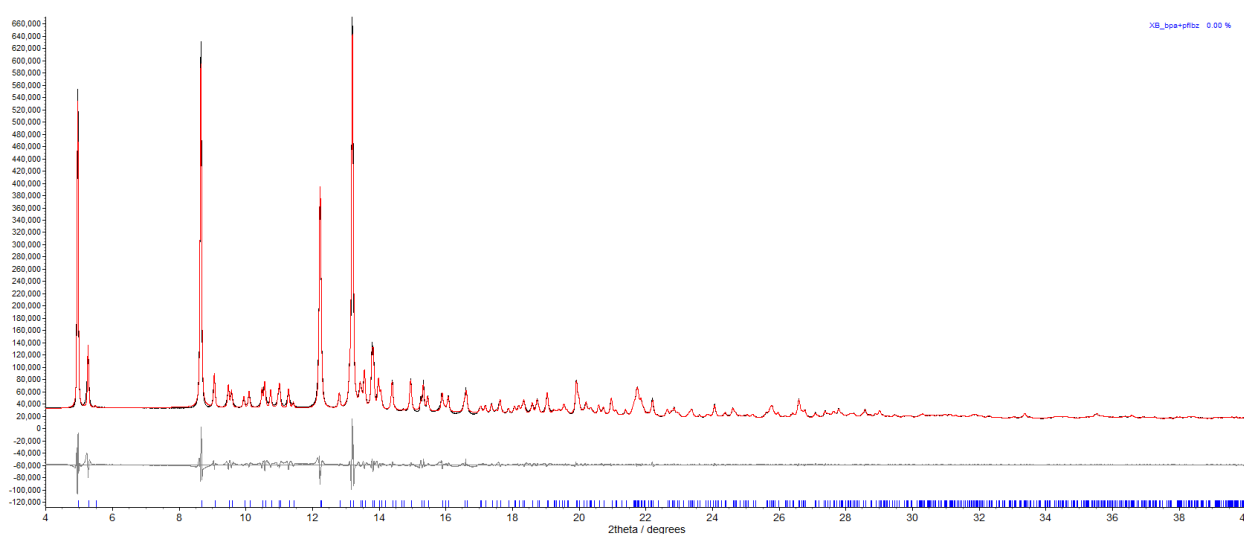


Figure S10.5. Observed (black) and calculated (red) profiles and difference plot [$I_{\text{obs}} - I_{\text{calc}}$] (grey) of the Pawley refinement. (2θ range 4.0 - 40 °, $d_{\text{min}} = 1.21 \text{ \AA}$).

System A: Competition experiment in nitromethane.

X-ray diffraction data of the white microcrystalline powder were collected using synchrotron radiation ($\lambda = 0.82665$ (1) Å). The pattern was compared with calculated X-ray powder patterns for **1•3** (the halogen-bonded co-crystal phase) for which the crystal structure was already established from single-crystal X-ray diffraction (CSD refcode MEKW00).^{S10} The unit cell parameters of **1•3** were used as a starting point for Pawley refinement,^{S5} employing 1304 parameters (8 background, 1 zero error, 5 profile, 6 cell, 1284 reflections). Pawley refinement converged to $R_{wp} = 0.0417$, $R_{wp}' = 0.0989$. [$a = 5.04113$ (4) Å, $b = 9.90950$ (8) Å, $c = 10.62338$ (8) Å, $\alpha = 64.7527$ (6) °, $\beta = 82.1148$ (7) °, $\gamma = 87.7556$ (6) °, $V = 475.328$ (7) Å³].

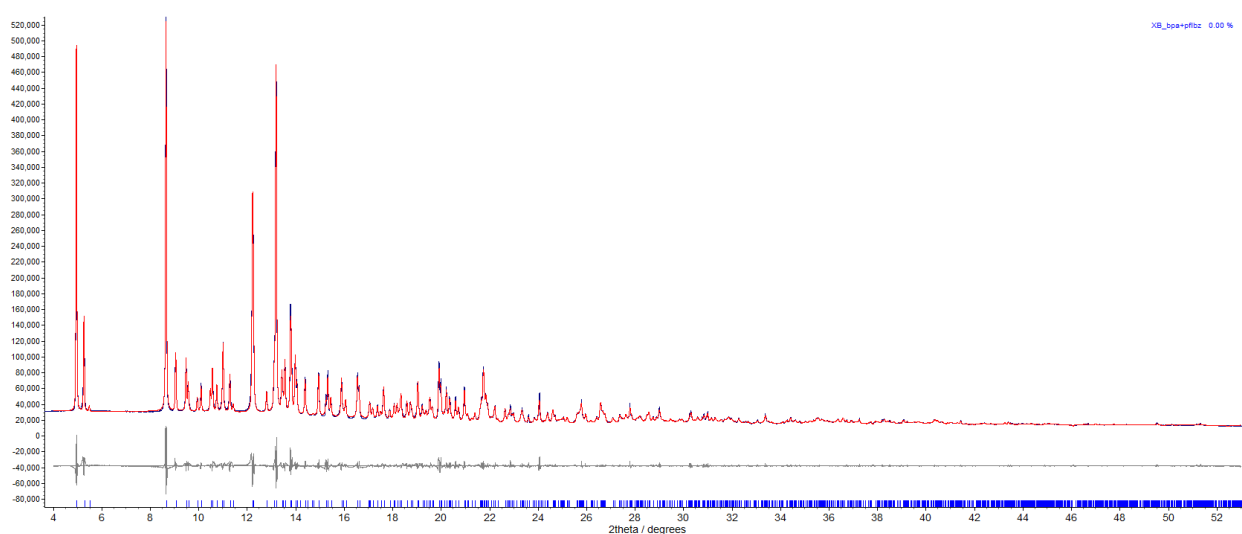


Figure S10.6. Observed (blue) and calculated (red) profiles and difference plot [$I_{\text{obs}} - I_{\text{calc}}$] (grey) of the Pawley refinement. (2θ range 4.0 - 53 °, $d_{\text{min}} = 0.93$ Å).

System A: Competition experiment in isopropanol

X-ray diffraction data of the white microcrystalline powder were collected using synchrotron radiation ($\lambda = 0.82665$ (1) Å). The pattern was compared with calculated X-ray powder patterns for **1•3** (the halogen-bonded co-crystal phase) for which the crystal structure was already established from single-crystal X-ray diffraction (CSD refcode MEKWO).^{S10} The unit cell parameters of **1•3** were used as a starting point for Pawley refinement,^{S5} employing 611 parameters (6 background, 1 zero error, 5 profile, 6 cell, 593 reflections). Pawley refinement converged to $R_{wp} = 0.0497$, $R_{wp}' = 0.1097$. [$a = 5.04155$ (7) Å, $b = 9.9110$ (2) Å, $c = 10.6242$ (1) Å, $\alpha = 64.772$ (1) °, $\beta = 82.097$ (1) °, $\gamma = 87.834$ (1) °, $V = 475.53$ (1) Å³].

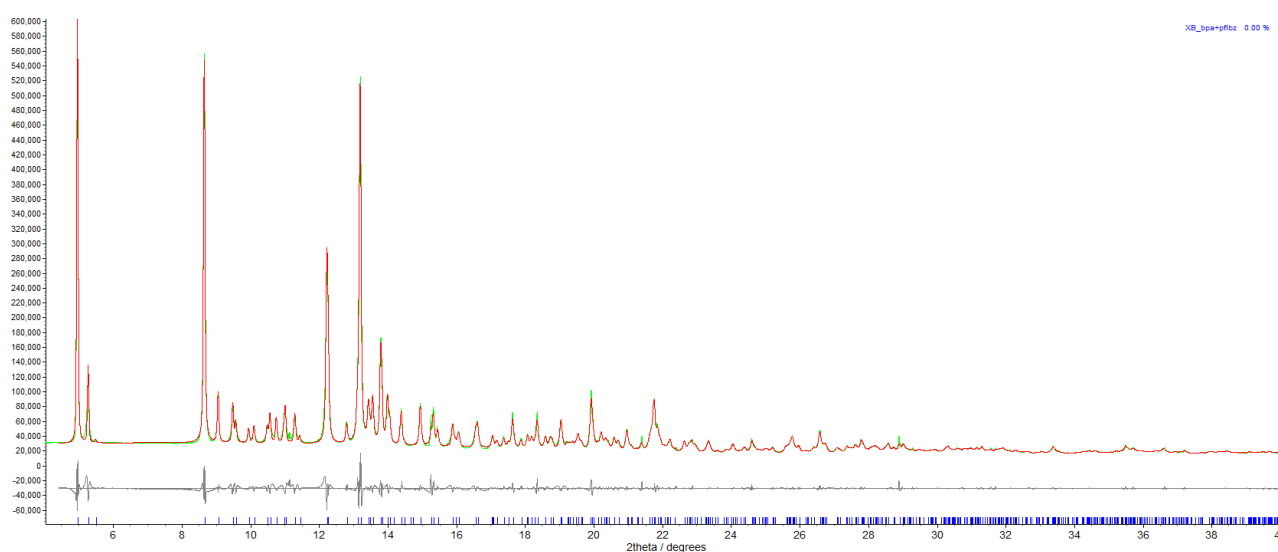
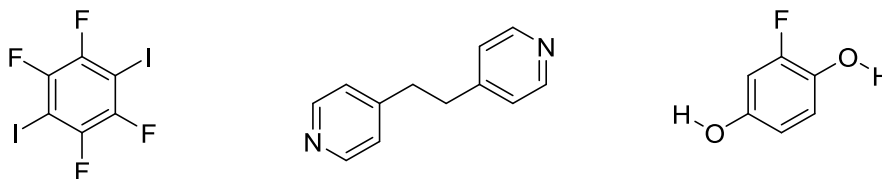


Figure S10.7. Observed (green) and calculated (red) profiles and difference plot [$I_{\text{obs}} - I_{\text{calc}}$] (grey) of the Pawley refinement. (2θ range 4.4 - 40 °, $d_{\text{min}} = 1.21$ Å).

11. Determination of Product Composition by XRPD: System B

[perfluoro-1,4-diiodobenzene (**1**), fluoroquinone (**2b**) and 1,2-bis(4-pyridyl)ethane (**3**)]



The X-ray powder diffraction patterns of the microcrystalline products from all competition experiments were recorded. These were compared to the calculated X-ray powder diffraction patterns for the hydrogen-bonded (**2b•3**) and halogen-bonded (**1•3**) co-crystals as well as the individual components (**1**, **2b** and **3**), before conducting quantitative fitting of the data.

System B: Competition experiment in toluene

X-ray diffraction data of the white microcrystalline powder was collected using Cu K α radiation. The pattern was compared with experimental X-ray powder pattern for **2b•3** (hydrogen-bonded co-crystal). The unit cell parameters of **2b•3** were used as a starting point for Pawley refinement,^{S5} employing 442 parameters (10 background, 1 zero error, 5 profile, 6 cell, 420 reflections). Pawley refinement converged to $R_{wp} = 0.0403$, $R_{wp'} = 0.0751$. [$a = 7.4247$ (5) Å, $b = 9.4115$ (6) Å, $c = 11.9308$ (8) Å, $\alpha = 96.005$ (5) °, $\beta = 92.493$ (6) °, $\gamma = 108.253$ (4) °, $V = 784.83$ (9) Å³].

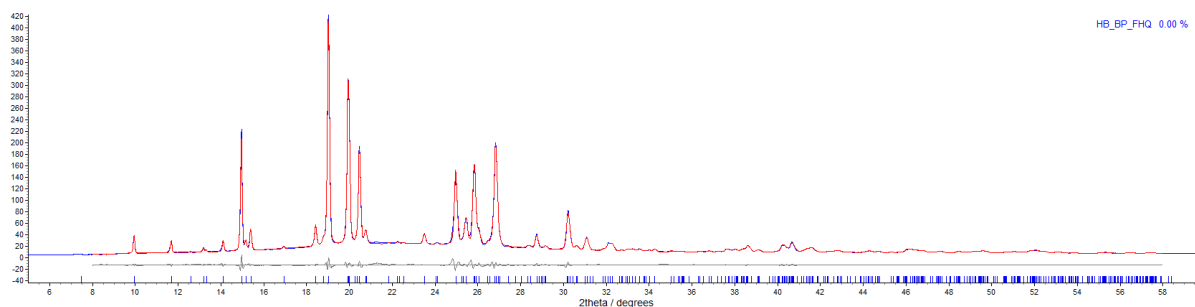


Figure S11.1. Observed (blue) and calculated (red) profiles and difference plot [$I_{\text{obs}} - I_{\text{calc}}$] (grey) of the Pawley refinement. (2θ range 8.0 - 58 °, $d_{\text{min}} = 1.59$ Å).

System B: Competition experiment in chloroform

X-ray diffraction data of the white microcrystalline powder was collected using Cu K α radiation. The pattern was compared with experimental X-ray powder pattern for **2b•3** (hydrogen-bonded co-crystal). The unit cell parameters of **2b•3** were used as a starting point for Pawley refinement,^{S5} employing 431 parameters (10 background, 1 zero error, 5 profile, 6 cell, 409 reflections). Pawley refinement converged to $R_{wp} = 0.0479$, $R_{wp}' = 0.0768$. [$a = 7.4250$ (1) Å, $b = 9.4097$ (1) Å, $c = 11.9293$ (2) Å, $\alpha = 96.005$ (2) °, $\beta = 92.476$ (2) °, $\gamma = 108.248$ (1) °, $V = 784.66$ (2) Å³].

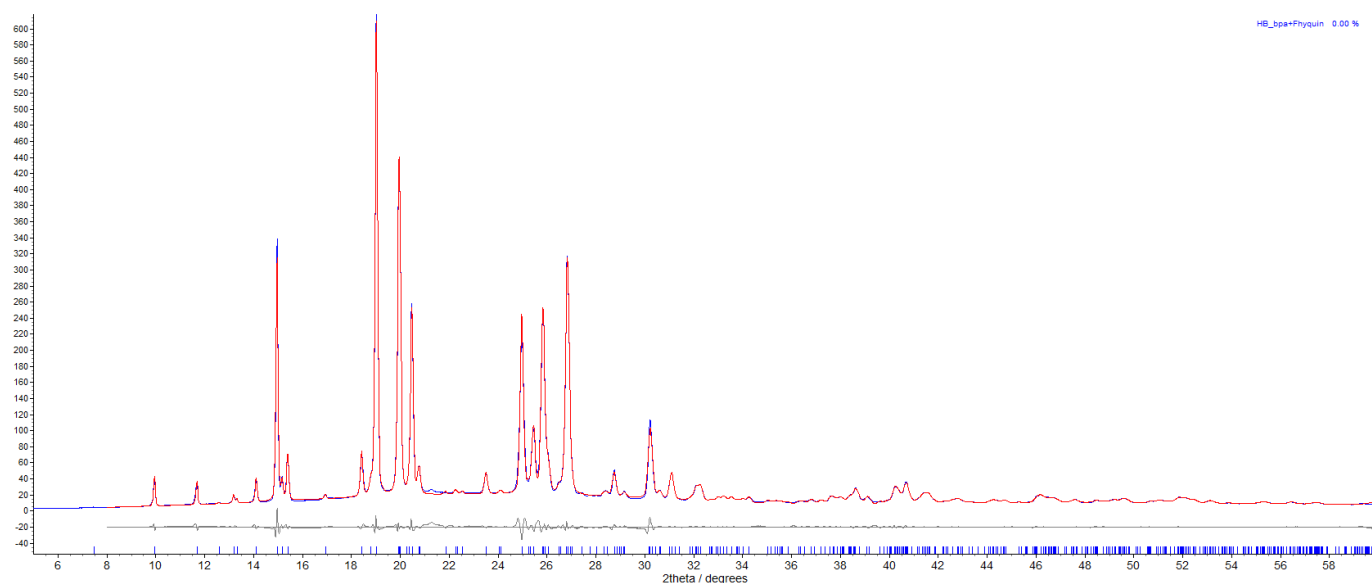


Figure S11.2. Observed (blue) and calculated (red) profiles and difference plot [$I_{\text{obs}} - I_{\text{calc}}$] (grey) of the Pawley refinement. (2θ range 8.0 - 60 °, $d_{\text{min}} = 1.54$ Å).

System B: Competition experiment in dichloromethane

X-ray diffraction data of the white microcrystalline product were collected using Cu K α radiation. The pattern was compared with experimental X-ray powder patterns for **2b•3** (hydrogen-bonded co-crystal) and for **1•3** (halogen-bonded co-crystal). The unit cell parameters of **1•3** and **2b•3** were used as a starting point for a mixed-phase Pawley refinement,^{S5} employing 703 parameters (10 background, 1 zero error, 9 profile, 12 cell, 671 reflections), resulting in final indices of fit $R_{wp} = 0.0441$, $R_{wp}' = 0.0744$. The starting model used for the mixed-phase Rietveld refinement,^{S11} conducted using TOPAS, used atomic coordinates from the single-crystal structures of **1•3** and **2b•3**. Refinement employed 36 parameters (10 background, 1 zero error, 9 profile, 12 cell, 2 scale, 2 global scale factors for thermal parameters). Rietveld refinement converged to $R_{wp} = 0.0751$, $R_{wp}' = 0.1333$. The relative phase amounts were found to be 95.25 (4) % of **2b•3** and 4.75 (4) % of **1•3**. [Unit cell parameters for **2b•3**: $a = 7.4265$ (2) Å, $b = 9.4132$ (2) Å, $c = 11.9356$ (5) Å, $\alpha = 96.031$ (6) °, $\beta = 92.498$ (6) °, $\gamma = 108.290$ (3) °, $V = 785.25$ (5) Å³; unit cell parameters for **1•3**: $a = 5.0399$ (4) Å, $b = 9.9183$ (8) Å, $c = 10.6230$ (7) Å, $\alpha = 64.770$ (5) °, $\beta = 82.139$ (6) °, $\gamma = 87.914$ (6) °, $V = 475.70$ (6) Å³].

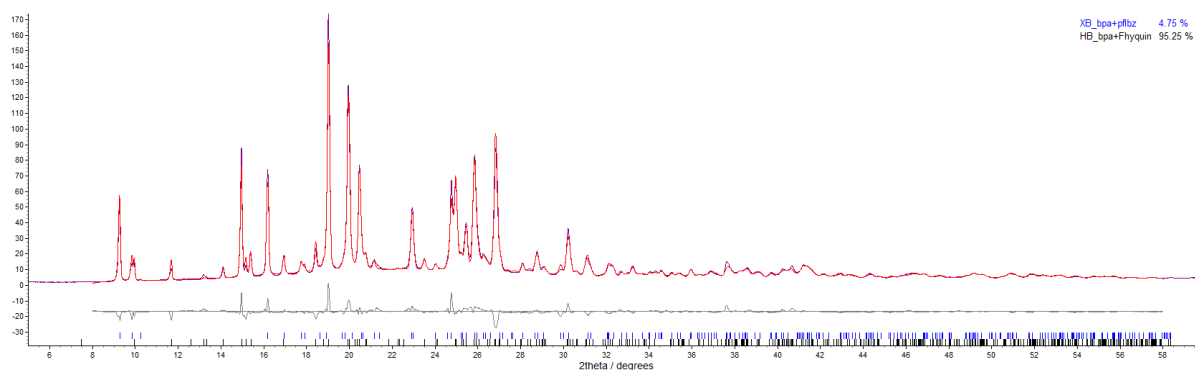


Figure S11.3. Observed (purple) and calculated (red) profiles and difference plot [$I_{\text{obs}} - I_{\text{calc}}$] (grey) of the Rietveld refinement. (2θ range 8.0 - 58 °, $d_{\text{min}} = 1.59$ Å).

System B: Competition experiment in acetone

X-ray diffraction data of the white microcrystalline powder was collected using Cu K α radiation. The pattern was compared with experimental X-ray powder pattern for **1•3** (halogen-bonded co-crystal). The unit cell parameters of **1•3** were used as a starting point for Pawley refinement,^{S5} employing 306 parameters (12 background, 1 zero error, 5 profile, 6 cell, 282 reflections). Pawley refinement converged to $R_{wp} = 0.0316$, $R_{wp}' = 0.1213$. [$a = 5.0380$ (2) Å, $b = 9.9020$ (4) Å, $c = 10.6163$ (4) Å, $\alpha = 64.783$ (2)°, $\beta = 82.105$ (3)°, $\gamma = 87.864$ (3)°, $V = 474.46$ (3) Å³].

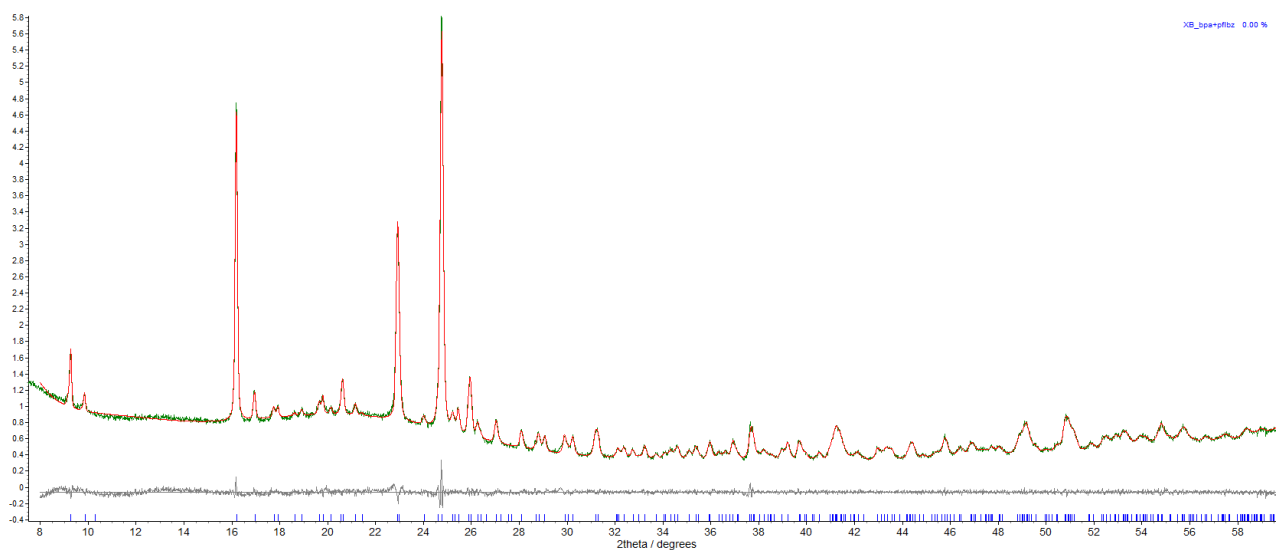


Figure S11.4. Observed (green) and calculated (red) profiles and difference plot [$I_{\text{obs}} - I_{\text{calc}}$] (grey) of the Pawley refinement. (2θ range 8.0 - 60°, $d_{\text{min}} = 1.54$ Å).

System B: Competition experiment acetonitrile

X-ray diffraction data of the white microcrystalline powder was collected using Cu K α radiation. The pattern was compared with experimental X-ray powder pattern for **1•3** (halogen-bonded co-crystal). The unit cell parameters of **1•3** were used as a starting point for Pawley refinement,^{S5} employing 302 parameters (10 background, 1 zero error, 5 profile, 6 cell, 280 reflections). Pawley refinement converged to $R_{wp} = 0.0518$, $R_{wp}' = 0.1442$. [$a = 5.0392$ (2) Å, $b = 9.9007$ (3) Å, $c = 10.6171$ (3) Å, $\alpha = 64.806$ (2)°, $\beta = 82.153$ (3)°, $\gamma = 87.881$ (3)°, $V = 474.70$ (3) Å³].

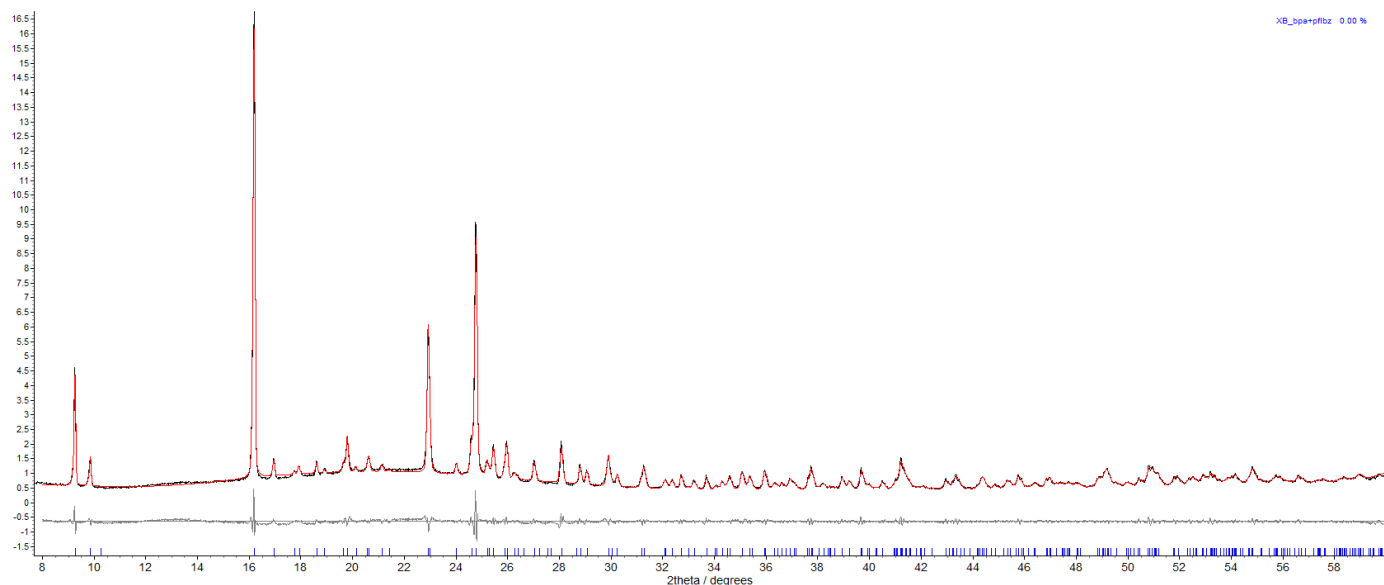


Figure S11.5. Observed (black) and calculated (red) profiles and difference plot [$I_{\text{obs}} - I_{\text{calc}}$] (grey) of the Pawley refinement. (2θ range 8.0 - 60°, $d_{\text{min}} = 1.54$ Å).

System B: Competition experiment in nitromethane

X-ray diffraction data of the white microcrystalline powder were collected using Cu K α radiation. The pattern was compared with experimental X-ray powder pattern for **1•3** (halogen-bonded co-crystal). The unit cell parameters of **1•3** were used as a starting point for Pawley refinement,^{S5} employing 302 parameters (10 background, 1 zero error, 5 profile, 6 cell, 280 reflections). Pawley refinement converged to $R_{wp} = 0.0372$, $R_{wp}' = 0.0929$. [$a = 5.0383$ (1) Å, $b = 9.9096$ (3) Å, $c = 10.620$ (2) Å, $\alpha = 64.785$ (2) °, $\beta = 82.142$ (2) °, $\gamma = 87.900$ (2) °, $V = 475.07$ (2) Å³].

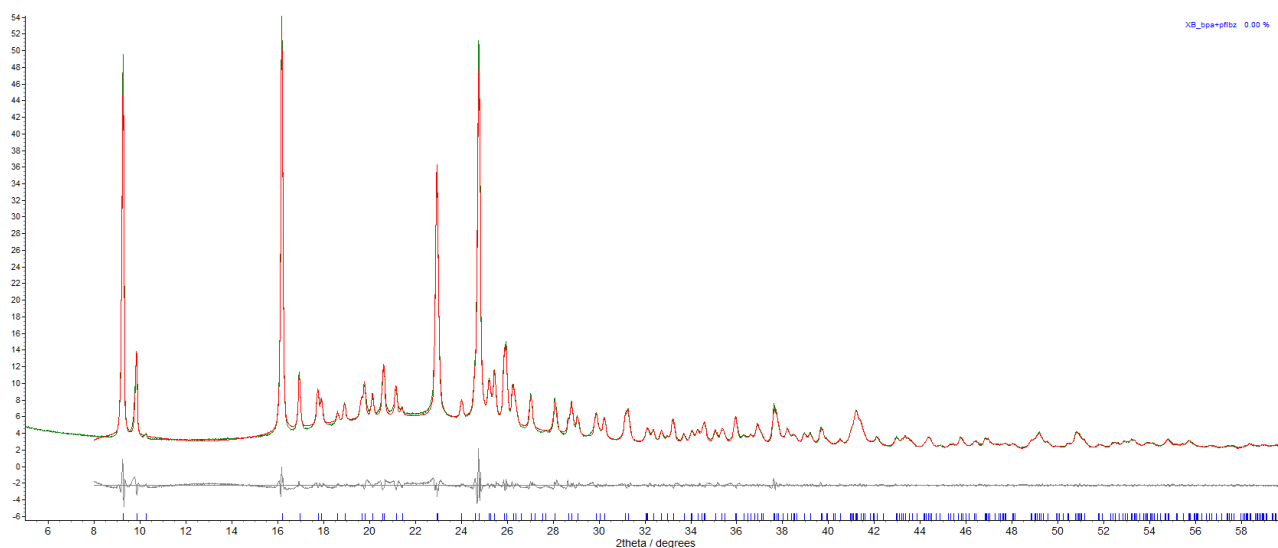


Figure S11.6. Observed (green) and calculated (red) profiles and difference plot [$I_{\text{obs}} - I_{\text{calc}}$] (grey) of the Pawley refinement. (2θ range 8.0 - 60 °, $d_{\text{min}} = 1.54$ Å).

System B: Competition experiment in isopropanol

X-ray diffraction data of the white microcrystalline powder were collected using Cu K α radiation. The pattern was compared with experimental X-ray powder pattern for **1•3** (halogen-bonded co-crystal). The unit cell parameters of **1•3** were used as a starting point for Pawley refinement,^{S5} employing 301 parameters (10 background, 1 zero error, 5 profile, 6 cell, 279 reflections). Pawley refinement converged to $R_{wp} = 0.0387$, $R_{wp}' = 0.1003$. [$a = 5.0393$ (2) Å, $b = 9.9051$ (3) Å, $c = 10.6223$ (3) Å, $\alpha = 64.792$ (2)°, $\beta = 82.146$ (2)°, $\gamma = 87.875$ (2)°, $V = 475.08$ (2) Å³].

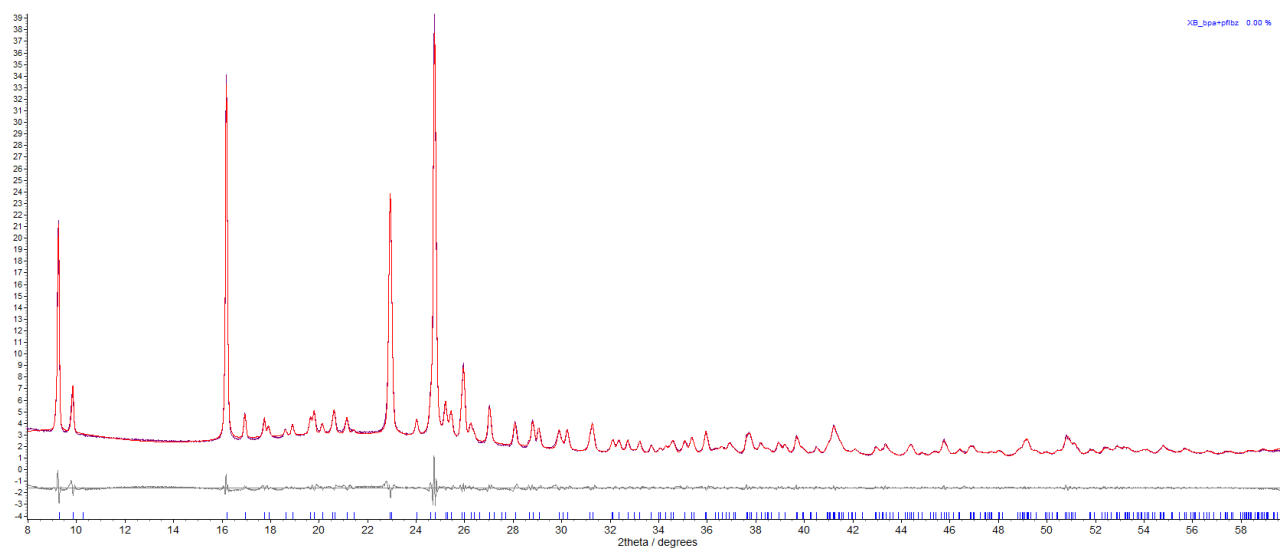
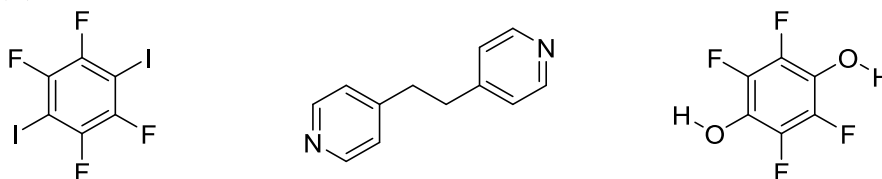


Figure S11.7. Observed (purple) and calculated (red) profiles and difference plot [$I_{\text{obs}} - I_{\text{calc}}$] (grey) of the Pawley refinement. (2θ range 8.0 - 60°, $d_{\text{min}} = 1.54$ Å).

12. Determination of Product Composition by XRPD: System C

[perfluoro-1,4-diiodobenzene (1), perfluorohydroquinone (2c) and 1,2-bis(4-pyridyl)ethane (3)]



The X-ray powder diffraction patterns of the microcrystalline products from all competition experiments were recorded. These were compared to the calculated X-ray powder diffraction patterns for the hydrogen-bonded (2c•3) and halogen-bonded (1•3) co-crystals as well as the individual components (1, 2c and 3), before conducting quantitative fitting of the data.

System C: Competition experiment in toluene.

X-ray diffraction data for the white microcrystalline product were collected using Cu K α radiation. The pattern was compared with experimental X-ray powder patterns for 2c•3 (the hydrogen-bonded co-crystal phase). The unit cell parameters of 2c•3 were used as a starting point for this Pawley refinement,^{S5} employing 257 parameters (14 background, 1 zero error, 5 profile, 6 cell, 277 reflections). Pawley refinement converged to $R_{wp} = 0.0364$, $R_{wp}' = 0.1068$. [$a = 6.3532(3) \text{ \AA}$, $b = 7.4422(3) \text{ \AA}$, $c = 9.2290(4) \text{ \AA}$, $\alpha = 86.129(3)^\circ$, $\beta = 75.975(3)^\circ$, $\gamma = 71.253(3)^\circ$, $V = 400.86(3) \text{ \AA}^3$].

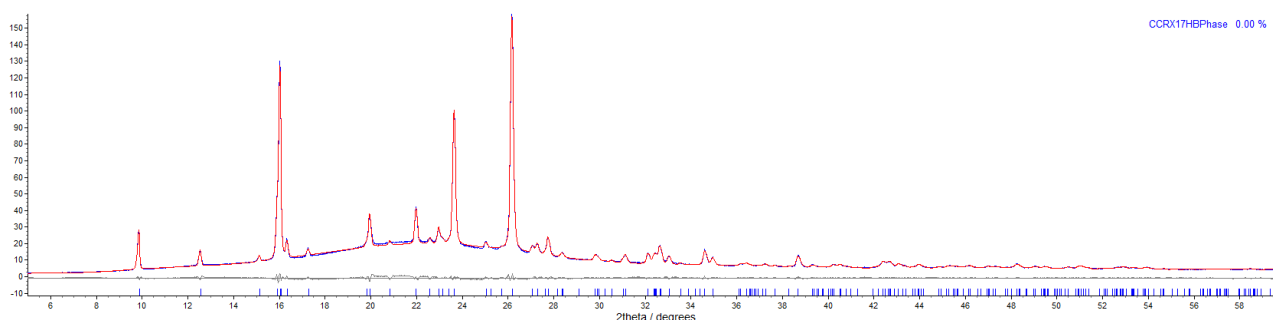


Figure S12.1. Observed (blue) and calculated (red) profiles and difference plot [$I_{\text{obs}} - I_{\text{calc}}$] (grey) of the Pawley refinement. (2θ range 5 - 60 $^\circ$, $d_{\text{min}} = 1.54 \text{ \AA}$).

System C: Competition experiment in Chloroform.

X-ray diffraction data for the white microcrystalline product were collected using Cu K α radiation. The pattern was compared with experimental X-ray powder patterns for **2c•3** (the hydrogen-bonded co-crystal phase). The unit cell parameters of **2c•3** were used as a starting point for this Pawley refinement,^{S5} employing 256 parameters (13 background, 1 zero error, 5 profile, 6 cell, 277 reflections). Pawley refinement converged to $R_{wp} = 0.0344$, $R_{wp}' = 0.0707$. [$a = 6.3536$ (3) Å, $b = 7.4426$ (1) Å, $c = 9.2272$ (2) Å, $\alpha = 86.142$ (1) °, $\beta = 75.800$ (1) °, $\gamma = 71.296$ (1) °, $V = 400.98$ (1) Å³].

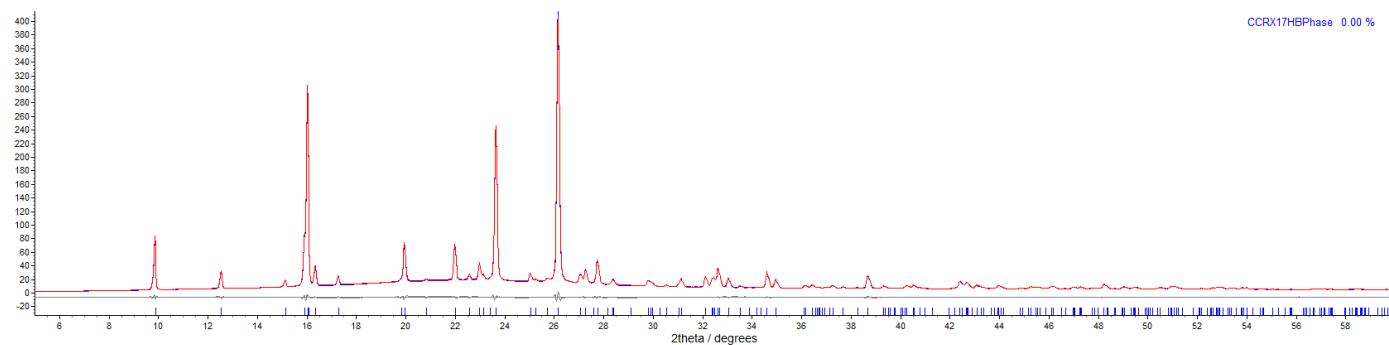


Figure S12.2. Observed (blue) and calculated (red) profiles and difference plot [$I_{\text{obs}} - I_{\text{calc}}$] (grey) of the Pawley refinement. (2θ range 5 - 60 °, $d_{\text{min}} = 1.54$ Å).

System C: Competition experiment in dichloromethane.

X-ray diffraction data for the white microcrystalline product were collected using Cu K α radiation. The pattern was compared with experimental X-ray powder patterns for **2c•3** (the hydrogen-bonded co-crystal phase). The unit cell parameters of **2c•3** were used as a starting point for this Pawley refinement,^{S5} employing 256 parameters (13 background, 1 zero error, 5 profile, 6 cell, 277 reflections). Pawley refinement converged to $R_{wp} = 0.0380$, $R_{wp}' = 0.0756$. [$a = 6.3552$ (2) Å, $b = 7.4409$ (2) Å, $c = 9.2310$ (2) Å, $\alpha = 86.124$ (1) °, $\beta = 75.993$ (1) °, $\gamma = 71.238$ (2) °, $V = 401.00$ (2) Å³].

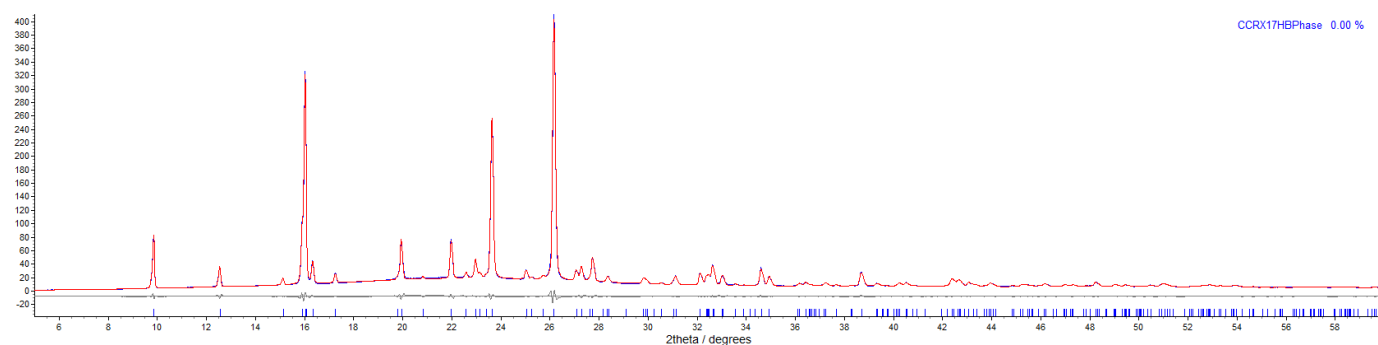


Figure S12.3. Observed (blue) and calculated (red) profiles and difference plot [$I_{\text{obs}} - I_{\text{calc}}$] (grey) of the Pawley refinement. (2θ range 5 - 60 °, $d_{\text{min}} = 1.54$ Å).

System C: Competition experiment in acetone

X-ray diffraction data for the white microcrystalline product were collected using Cu K α radiation. The pattern was compared with experimental X-ray powder patterns for **2c•3** (the hydrogen-bonded co-crystal phase). The unit cell parameters of **2c•3** were used as a starting point for this Pawley refinement,^{S5} employing 256 parameters (12 background, 1 zero error, 5 profile, 6 cell, 232 reflections). Pawley refinement converged to $R_{wp} = 0.0477$, $R_{wp}' = 0.0990$. [$a = 6.3571$ (3) Å, $b = 7.4374$ (3) Å, $c = 9.2277$ (4) Å, $\alpha = 86.167$ (3) °, $\beta = 76.087$ (4) °, $\gamma = 71.354$ (3) °, $V = 401.23$ (3) Å³].

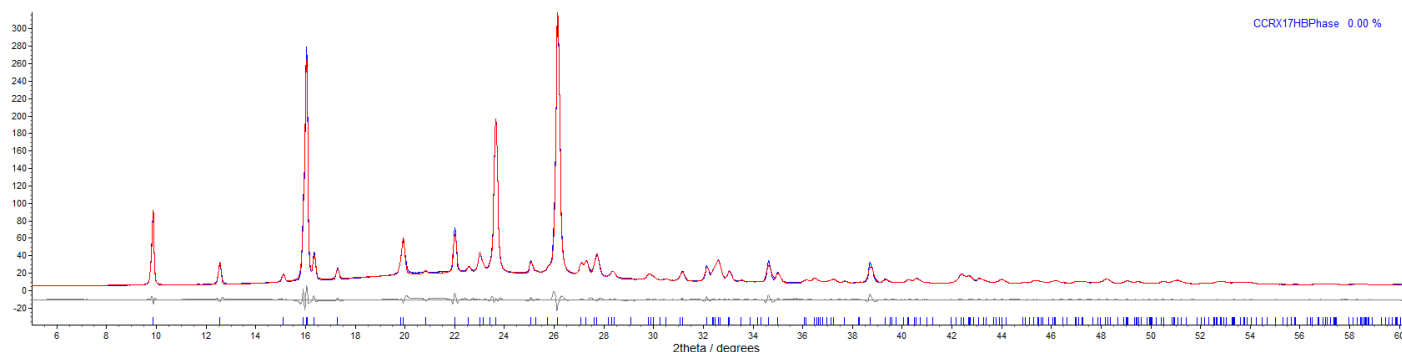


Figure S12.4. Observed (blue) and calculated (red) profiles and difference plot [$I_{\text{obs}} - I_{\text{calc}}$] (grey) of the Pawley refinement. (2θ range 5 - 60 °, $d_{\text{min}} = 1.54$ Å).

System C: Competition in acetonitrile

X-ray diffraction data for the white microcrystalline product were collected using Cu K α radiation. The pattern was compared with experimental X-ray powder patterns for **2c•3** (the hydrogen-bonded co-crystal phase). The unit cell parameters of **2c•3** were used as a starting point for this Pawley refinement,^{S5} employing 256 parameters (12 background, 1 zero error, 5 profile, 6 cell, 232 reflections). Pawley refinement converged to $R_{wp} = 0.0369$, $R_{wp}' = 0.1622$. [$a = 6.3603$ (2) Å, $b = 7.4371$ (2) Å, $c = 9.2348$ (2) Å, $\alpha = 86.109$ (2) °, $\beta = 76.028$ (2) °, $\gamma = 71.216$ (2) °, $V = 401.30$ (2) Å³].

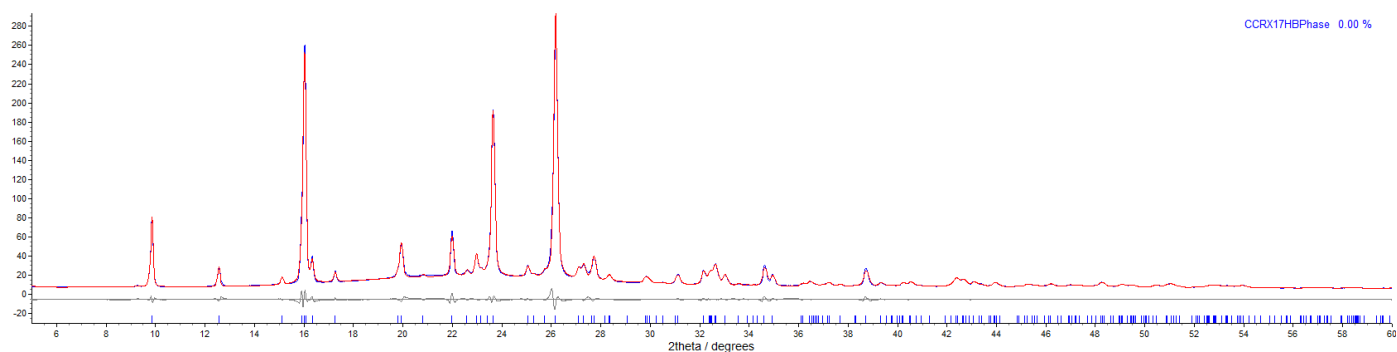


Figure S12.5. Observed (blue) and calculated (red) profiles and difference plot [$I_{\text{obs}} - I_{\text{calc}}$] (grey) of the Pawley refinement. (2θ range 5 - 60 °, $d_{\text{min}} = 1.54$ Å).

System C: Competition experiment in nitromethane

X-ray diffraction data for the white microcrystalline product were collected using Cu K α radiation. The pattern was compared with experimental X-ray powder patterns for **2c•3** (the hydrogen-bonded co-crystal phase). The unit cell parameters of **2c•3** were used as a starting point for this Pawley refinement,^{S5} employing 255 parameters (12 background, 1 zero error, 5 profile, 6 cell, 277 reflections). Pawley refinement converged to $R_{wp} = 0.0343$, $R_{wp}' = 0.0754$. [$a = 6.3561$ (1) Å, $b = 7.4401$ (1) Å, $c = 9.2312$ (2) Å, $\alpha = 86.121$ (1)°, $\beta = 75.994$ (1)°, $\gamma = 71.228$ (1)°, $V = 401.001$ (1) Å³].

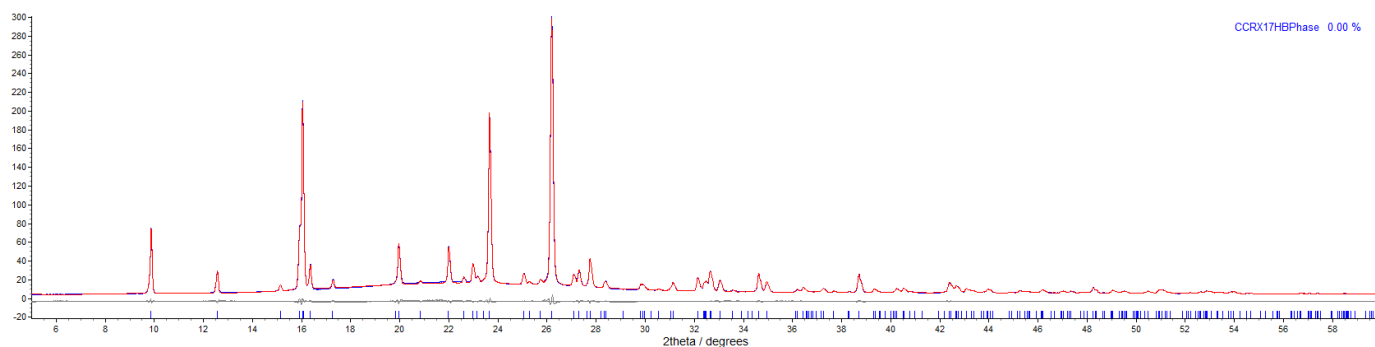


Figure S12.6. Observed (blue) and calculated (red) profiles and difference plot [$I_{obs} - I_{calc}$] (grey) of the Pawley refinement. (2θ range 5 - 60°, $d_{min} = 1.54$ Å).

System C: Competition experiment in isopropanol

X-ray diffraction data of the white microcrystalline product were collected using Cu K α radiation. The pattern was compared with experimental X-ray powder patterns for **2c•3** (hydrogen-bonded co-crystal) and for **1•3** (halogen-bonded co-crystal). The unit cell parameters of **1•3** and **2c•3** were used as a starting point for a mixed-phase Pawley refinement,^{S5} employing 546 parameters (12 background, 1 zero error, 9 profile, 12 cell, 512 reflections), resulting in final indices of fit $R_{wp} = 0.0297$, $R_{wp}' = 0.0615$. The starting model used for the mixed-phase Rietveld refinement,^{S11} conducted using TOPAS, used atomic coordinates from the single-crystal structures of **1•3** and **2c•3**. Refinement employed 38 parameters (12 background, 1 zero error, 9 profile, 12 cell, 2 scale, 2 global thermal displacement scale factors). Rietveld refinement converged to $R_{wp} = 0.0845$, $R_{wp}' = 0.1550$. The relative phase amounts were found to be 69.3 (5) % of **2c•3** and 30.7 (5) % of **1•3**. [Unit cell parameters for **2c•3**: $a = 6.358$ (1) Å, $b = 7.431$ (2) Å, $c = 9.227$ (2) Å, $\alpha = 85.87$ (2) °, $\beta = 76.04$ (1) °, $\gamma = 71.20$ (2) °, $V = 400.5$ (2) Å³; unit cell parameters for **1•3**: $a = 5.0301$ (5) Å, $b = 9.9476$ (9) Å, $c = 10.622$ (1) Å, $\alpha = 64.749$ (6) °, $\beta = 82.020$ (7) °, $\gamma = 87.947$ (7) °, $V = 475.89$ (8) Å³].

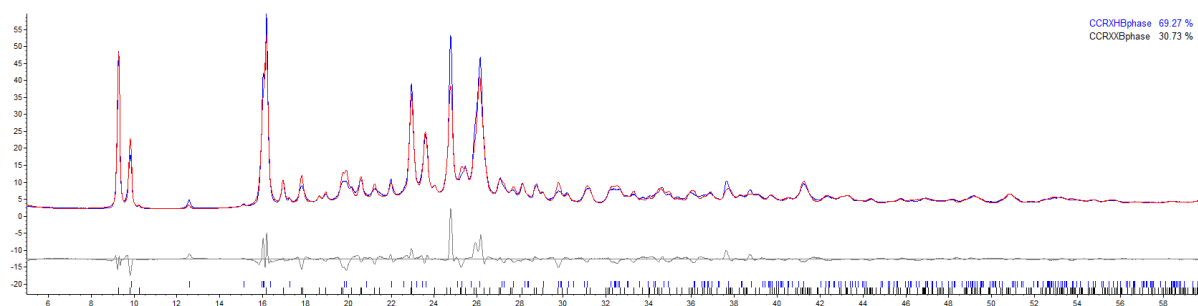


Figure S12.7. Observed (blue) and calculated (red) profiles and difference plot [$I_{\text{obs}} - I_{\text{calc}}$] (grey) of the Pawley refinement. (2θ range 5 - 60 °, $d_{\text{min}} = 1.54$ Å).

13. Single Crystal Diffraction Studies

Crystals were mounted on a mylar loop using a viscous hydrocarbon oil and transferred directly to the cold nitrogen stream at 100 K for data collection on either a Bruker SMART APEX-II CCD diffractometer operating with a Mo-K α sealed tube X-ray source or Bruker D8 VENTURE diffractometer equipped with the PHOTON 100 CMOS detector, using Cu-K α micro-focus X-ray source. For Bruker D8 VENTURE collections, intensity data were collected in shutterless mode, with a frame width of 0.5°, and a total exposure of 60 s per degree. A final fast scan was collected at lower incident beam intensity to enable correction for any detector saturation for low-angle data.

A summary of data collection and structure refinement information is provided in Table S3. Intensity data were corrected for absorption using empirical methods (SADABS) based upon symmetry equivalent reflections combined with measurements at different azimuthal angles.^{S12} The crystal structure was solved and refined against all F^2 values using the SHELXL^{S13} accessed via the Olex2 program.^{S14} Non-hydrogen atoms were refined anisotropically. Hydrogen atoms were placed in calculated positions with idealized geometries and then refined by employing a riding model and isotropic displacement parameters. Disordered fluorine and hydrogen atoms in **2b•3** were modelled by refinement of site occupancies.

Table S3. Data collection, structure solution and refinement parameters for crystal structures of 2b•3 and 2c•3

| | (2b•3) C ₆ H ₅ F(OH) ₂ •C ₁₂ H ₁₂ N ₂ | (2c•3) C ₆ F ₄ (OH) ₂ •C ₁₂ H ₁₂ N ₂ |
|---|--|---|
| Crystal habit | Block | Plate |
| Crystal colour | Colourless | Colourless |
| Crystal size (mm) | 0.14 x 0.12 x 0.02 | 0.20 x 0.20 x 0.050 |
| Crystal system | Triclinic | Triclinic |
| Space group, <i>Z</i> | <i>P</i> -1, 2 | <i>P</i> -1, 1 |
| <i>a</i> (Å) | 7.1389(13) | 6.1939(4) |
| <i>b</i> (Å) | 9.2830(15) | 7.4692(5) |
| <i>c</i> (Å) | 11.8655(16) | 9.0672(6) |
| α (°) | 95.669(10) | 86.863(5) |
| β (°) | 91.769(11) | 75.722(5) |
| γ (°) | 107.117(13) | 71.755(4) |
| <i>V</i> (Å ³) | 749.5(2) | 385.97(5) |
| Wavelength (Å) | 1.54178 | 0.71073 |
| Density (Mg m ⁻³) | 1.384 | 1.576 |
| Temperature (K) | 100 | 100 |
| μ (mm ⁻¹) | 0.822 | 0.136 |
| θ range (°) | 3.751 to 66.961 | 2.318 to 27.562 |
| Reflns. collected | 7125 | 6725 |
| Independent reflns. (<i>R</i> _{int}) | 2511 (0.0690) | 1778 (0.0313) |
| Reflns. used in refinement, <i>n</i> | 2511 | 1778 |
| LS parameters, <i>p</i> | 219 | 119 |
| Restraints, <i>r</i> | 0 | 0 |
| <i>R</i> 1 (<i>F</i>) ^a <i>I</i> > 2.0 σ (<i>I</i>) | 0.0700 | 0.0388 |
| <i>wR</i> 2 (<i>F</i> ²) ^a , all data | 0.2097 | 0.0955 |
| <i>S</i> (<i>F</i> ²) ^a , all data | 1.018 | 1.022 |

14. References

- S1. S. P. Thompson, J. E. Parker, J. Potter, T. P. Hill, A. Birt, T. M. Cobb, F. Yuan and C. C. Tang, *Rev. Sci. Instrum.*, 2009, **80**, 075107.
- S2. S. P. Thompson, J. E. Parker, J. Marchal, J. Potter, A. Birt, F. Yuan, R. D. Fearn, A. R. Lennie, S. R. Street and C. C. Tang, *J. Synchrotron Rad.*, 2011, **18**, 637.
- S3. A. A. Coelho, *TOPAS Academic, Version 4.1*, 2007; see <http://www.topas-academic.net>.
- S4. S. Ide, N. Karacan, Y. Tufan, *Acta Crystallogr.*, 1995, **C51**, 2304.
- S5. G. S. Pawley, *J. Appl. Cryst.*, 1981, **14**, 357.
- S6. R. Boese, T. Miebach, Private communication to CCDC, 1996. Deposition number CSD320040.
- S7. S. C. Wallwork, H. M. Powell, *J. Chem. Soc. Perkin Trans.*, 1980, 641.
- S8. Carrington, E. C.; Robertson, C. C.; Brammer, L. unpublished results. The crystal structure will be reported in a separate publication.
- S9. V. R. Thalladi, H.-C. Weiss, R. Boese, A. Nangia, G. R. Desiraju, *Acta Crystallogr.*, 1999, **B55**, 1005.
- S10. E. Corradi, S. V. Meille, M. T. Messina, P. Metrangolo, G. Resnati, *Angew. Chem. Int. Ed.*, 2000, **39**, 1782.
- S11. H. M. Rietveld, *J. Appl. Crystallogr.*, 1969, **2**, 65.
- S12. L. Krause, R. Herbst-Irmer, G. M. Sheldrick, D. Stalke, *J. Appl. Cryst.*, 2015, **48**, 3.
- S13. G. M. Sheldrick, *Acta Crystallogr.*, 2015, **C71**, 3.
- S14. O.V. Dolomanov, L. J. Bourhis, R. J. Gildea, J. A. K. Howard, H. Puschmann, *J. Appl. Cryst.*, 2009, **42**, 339.

Cite this: *Chem. Sci.*, 2017, 8, 5392

Hydrogen bonding vs. halogen bonding: the solvent decides†

Craig C. Robertson,^a James S. Wright,^a Elliot J. Carrington,^{‡a}
Robin N. Perutz,^{*b} Christopher A. Hunter^{*c} and Lee Brammer^{*a}

Control of intermolecular interactions is integral to harnessing self-assembly in nature. Here we demonstrate that control of the competition between hydrogen bonds and halogen bonds, the two most highly studied directional intermolecular interactions, can be exerted by choice of solvent (polarity) to direct the self-assembly of co-crystals. Competitive co-crystal formation has been investigated for three pairs of hydrogen bond and halogen bond donors, which can compete for a common acceptor group. These competitions have been examined in seven different solvents. Product formation has been determined and phase purity has been examined by analysis of powder X-ray diffraction patterns. Formation of hydrogen-bonded co-crystals is favoured from less polar solvents and halogen-bonded co-crystals from more polar solvents. The solvent polarity at which the crystal formation switches from hydrogen-bond to halogen-bond dominance depends on the relative strengths of the interactions, but is not a function of the solution-phase interactions alone. The results clearly establish that an appreciation of solvent effects is critical to obtain control of the intermolecular interactions.

Received 22nd April 2017
Accepted 17th May 2017

DOI: 10.1039/c7sc01801k

rsc.li/chemical-science

Introduction

Inspiration from molecular recognition and self-assembly processes in nature has led to the exploration of self-assembly in chemistry with a view to exerting synthetic control. Such efforts are central to prominent research fields such as supramolecular chemistry^{1,2} and crystal engineering,^{3,4} and are of increasing impact in areas such as materials chemistry⁵ and catalysis.⁶ Control of self-assembly processes remains highly challenging as a consequence of the relatively weak interactions involved. Most prominent of these interactions, both in naturally occurring systems and in synthetic assemblies, are hydrogen bonds (HBs), which are among the strongest and most directional of intermolecular interactions. Another class of important, directional intermolecular interactions are halogen bonds (XBs). Halogen bonds have come to prominence

over the past 15 years,^{7–10} and have been exploited in the fields of crystal engineering,^{11,12} soft matter,¹³ protein–ligand interactions,¹⁴ anion recognition and transport,^{15,16} catalysis¹⁷ and materials chemistry.^{18,19} Halogen bonds involve the interaction of a covalently-bound halogen atom, usually iodine, with an electron-rich region of a neighbouring atom or molecule. The halogen adopts a Lewis acidic role, exemplified by the region of positive electrostatic potential on the surface of the halogen, which lies *trans* to its σ -bond and is usually referred to as the σ -hole.²⁰ In this article we clearly demonstrate for the first time, using co-crystal formation as an exemplar, that appreciation of solvent properties is essential to control the outcome of direct competition between formation of hydrogen bonds and halogen bonds in self-assembly.

Understanding the role of specific intermolecular interactions in directing crystal growth is of particular interest in designing crystalline forms of commodity chemicals, such as pharmaceuticals,^{21,22} agrochemicals,²³ pigments²⁴ and energetic materials,^{25,26} whose physical properties depend on their solid form. Such forms include not only single phases and their polymorphs, but also solvates and, increasingly, co-crystals, which allow the inclusion of a variety of co-crystal former molecules to enable tuning of physical properties through changes in crystal structure. A number of approaches have been taken to understand the formation of co-crystals and enable development of new materials.²⁷ Computational approaches include crystal structure prediction (CSP), which is based on calculation of lattice enthalpies for putative crystal structures.^{28,29} Alternatively, interaction propensity calculations can

^aDepartment of Chemistry, University of Sheffield, Brook Hill, Sheffield, S3 7HF, UK. E-mail: lee.brammer@sheffield.ac.uk

^bDepartment of Chemistry, University of York, Heslington, York, YO10 5DD, UK. E-mail: robin.perutz@york.ac.uk

^cDepartment of Chemistry, University of Cambridge, Lensfield Road, Cambridge CB2 1EW, UK. E-mail: ch664@cam.ac.uk

† Electronic supplementary information (ESI) available: Full details of all experimental procedures and analysis of NMR spectroscopic data, powder X-ray data and single-crystal X-ray diffraction data. CCDC 1478819 and 1478820, for compounds **2b**·**3** and **2c**·**3** contain the supplementary crystallographic data for this paper. For ESI and crystallographic data in CIF or other electronic format see DOI: 10.1039/c7sc01801k

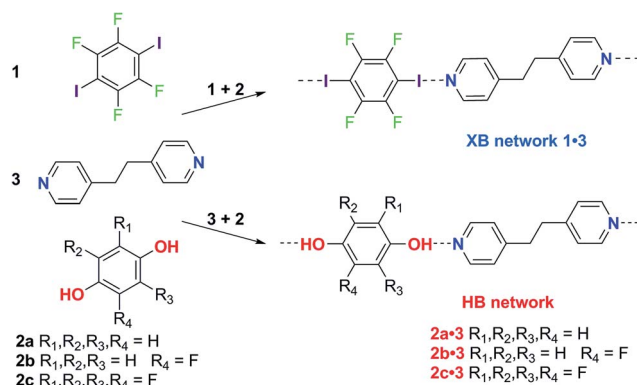
‡ Current address: Department of Chemistry, University of Liverpool, Liverpool L69 7ZD, UK.



be used to predict co-crystal formation based on likelihood of formation of intermolecular interactions,³⁰ principally hydrogen bonds, between available functional groups, and are based on knowledge from the large number of known crystal structures present in the Cambridge Structural Database.³¹ Experimental approaches may involve screening of a number of potential co-formers (molecules used to form co-crystals with a desired compound). Co-formers are selected based upon their likely formation of intermolecular interactions and screened in a series of co-crystallization experiments.^{32,33} Absent from most approaches is a specific consideration of the role of solvent in crystal structure formation although solvent effects on directing the crystallization of different polymorphs of molecular crystals have been observed.³⁴ One reason for this is the complexity of accounting for the kinetic and thermodynamic role of solvent in the methodology used, but another reason is a lack of understanding of its importance. The potential influence of solvent on solution-phase self-assembly, however, extends far beyond crystallization processes and improved control of molecular self-assembly remains a goal for supramolecular chemistry if we are to harness intermolecular interactions in the manner in which nature has evolved to do so.

The effect of solvent on hydrogen bonding in solution has been studied. Notably, the hydrogen bonding scale developed by Hunter quantitatively relates empirical hydrogen bond donor strength (α) and hydrogen bond acceptor strength (β) parameters to the free energy of interaction for the hydrogen bond in solution.³⁵ This model explicitly accounts for the role of the solvent by taking into account its hydrogen bond donor and acceptor strengths (α_s, β_s). Recently we have demonstrated that the strongly-bound halogen-bonded complex iodine·thiourea is stable in a wide range of solvent environments in contrast to hydrogen-bonding interactions, which may be strong in nonpolar solvents, but weak in polar solvents.³⁶ These results led us to consider more broadly the role of solvent in directing the competition between intermolecular interactions in the formation of crystals, and specifically co-crystals as a prominent exemplar of self-assembly. We chose the competition between hydrogen bonding and halogen bonding, the two most widely studied intermolecular interactions, for this investigation. The competition between 1,4-diodotetrafluorobenzene (**1**) and hydroquinone (**2a**) to form co-crystals with 1,2-bis(4-pyridyl)ethane (**3**) *via* halogen bonding or hydrogen bonding, respectively, was examined by Metrangolo, Resnati and coworkers.³⁷ Their report, showing that the halogen-bonded co-crystals **1·3** formed exclusively, in preference to the hydrogen-bonded co-crystals **2a·3**, when **1**, **2a** and **3** are dissolved in equimolar quantities in acetone, provided a starting point for our investigations.

Here we report a series of co-crystal formation experiments using halogen-bond donor **1** in competition with either hydrogen-bond donor **2a** or its monofluoro- or tetrafluoro-substituted analogues, **2b** and **2c**, respectively (Scheme 1). These studies were conducted in seven different solvents with **3** as the acceptor, forming a co-crystal in each case. Thus, we have examined hydrogen bond *vs.* halogen bond pairings of different relative interaction strengths and the role of solvent polarity in



Scheme 1 Synthesis of hydrogen-bonded (HB) and halogen-bonded (XB) co-crystals. Co-crystallization of XB donor **1** or HB donor **2** with 1,2-bis(4-pyridyl)ethane **3** to form the XB network **1·3** or HB network as **2·3**, respectively.

controlling the competition. In all cases the hydrogen-bonded co-crystals (**2·3**) are formed selectively in the least polar solvent, toluene, but formation of the halogen-bonded co-crystal (**1·3**) ultimately dominates as solvent polarity increases. These results are discussed in the context of solution-phase NMR titrations that determine hydrogen bond and halogen bond strengths, and demonstrate the critical role of solvent in tuning the competition between intermolecular interactions and controlling the form of the co-crystal product. The crossover point (in solvent polarity) between formation of the two crystalline products correlates with the relative strength of the halogen bonds and hydrogen bonds formed.

Results and discussion

Single crystals of the co-crystals **1·3** (XB network), **2a·3** (HB network), **2b·3** (HB) and **2c·3** (HB) were prepared separately by co-crystallization of each pair of components in acetone. The crystal structures of the four co-crystals establish that each comprises 1D networks in which the two molecular components alternate and are linked *via* either C–I···N halogen bonds (**1·3**) or O–H···N hydrogen bonds (**2a·3**, **2b·3** and **2c·3**). In each case the 1D networks adopt stacking arrangements of the aromatic rings in the two molecular components. Structure **1·3** is arranged in offset homomolecular stacks (Fig. 1a), structures **2a·3** and **2b·3** are isostructural and exhibit separate homomolecular and heteromolecular stacks (Fig. 1b and c), and **2c·3** exhibits stacks containing both homomolecular and heteromolecular interactions (Fig. 1d).

Having established the crystal structures of the possible co-crystals, bulk syntheses of each co-crystal were undertaken by co-crystallization of each pair of components from acetone. In each case Pawley fitting³⁸ of the resultant powder diffraction pattern established that the co-crystals form as the only crystalline product (see Section 9 of ESI†). Powder diffraction further established that the patterns for the hydrogen-bonded co-crystals **2·3** could be readily distinguished from those of the halogen-bonded co-crystal **1·3**, and that all co-crystals could



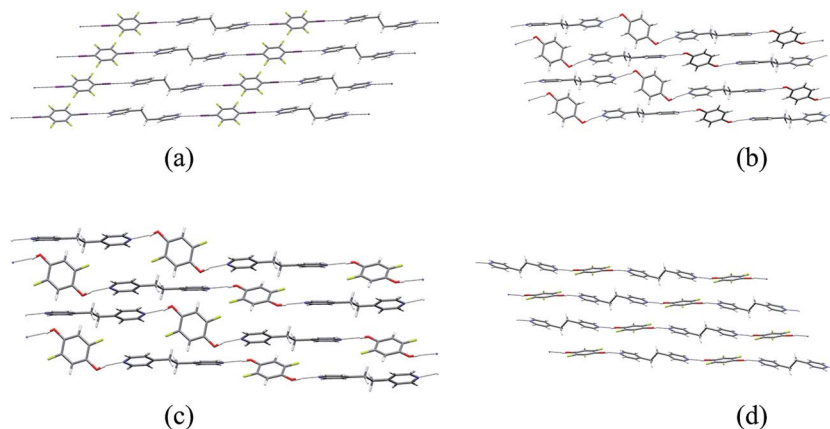


Fig. 1 Crystal structures of co-crystals: (a) XB network **1·3**, (b) HB network **2a·3**, (c) HB network **2b·3**, (d) HB network **2c·3**. The molecule of **2b** (in (c)) exhibits 50 : 50 F/H disorder at the 2- and 5-positions; disordered H atom sites are not shown. The crystal structures of **1·3** and **2a·3** have been previously reported³⁷ and are consistent with the structures determined herein.

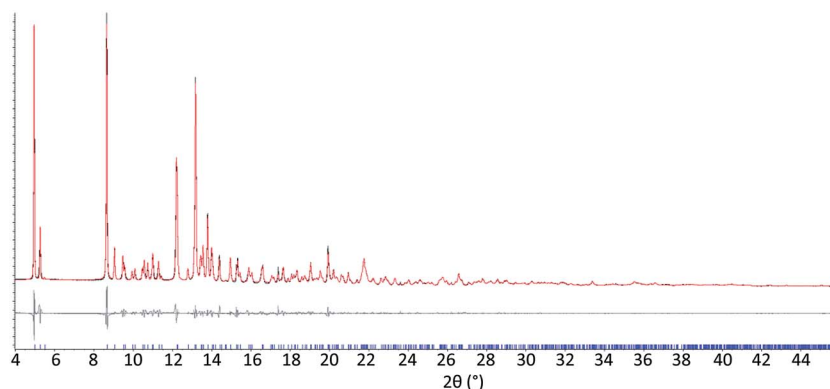


Fig. 2 Exclusive formation of halogen-bonded co-crystal **1·3** obtained from system A competitive co-crystallization in acetone. Observed (black) and calculated (red) powder X-ray diffraction profiles and difference plot [$I_{\text{obs}} - I_{\text{calc}}$] (grey) of the Pawley refinement showing the fit for co-crystal **1·3** as a single phase obtained from system A competitive co-crystallization in acetone (synchrotron radiation $\lambda = 0.82582(1)$ Å, $4.0 \leq 2\theta \leq 46.0^\circ$, $d_{\text{min}} = 1.06$ Å; $R_{\text{wp}} = 0.0511$, $R_{\text{wp}'} = 0.1143$).

be readily distinguished from crystals of the single molecular components (**1**, **2** and **3**).

Three competitive co-crystallization systems (**A**, **B** and **C**) were then investigated in which a halogen bond donor directly competes with a hydrogen bond donor to form co-crystals with a common acceptor molecule. 1,2-Bis(4-pyridyl)ethane **3** was used as the ditopic acceptor of hydrogen bonds or halogen bonds throughout all experiments. 1,4-Diiodotetrafluorobenzene **1** served as the ditopic XB donor and the strength of the competing HB donor was adjusted by using either hydroquinone **2a** (the weakest HB donor, used in system **A**), fluorohydroquinone **2b** (intermediate strength, system **B**) or tetrafluorohydroquinone **2c** (strongest HB donor, system **C**). The ranking of the hydrogen bond donor strengths was confirmed by solution-phase NMR spectroscopic titrations and is discussed in more detail below. An equimolar solution of **1**, **3**, and either **2a**, **2b** or **2c** was prepared in each of seven solvents and the solvent was allowed to evaporate slowly for 24 h at room temperature. The solid formed was isolated by filtration, dried and ground before characterization by powder X-ray diffraction.

Where the powder pattern could be indexed as a single phase, the phase purity of the product was established by Pawley refinement and where a mixture of products was identified upon indexing, mixed-phase Rietveld refinement³⁹ was conducted to establish the relative proportions of the products (see Sections 10–12 in ESI†).

The results from system **A** (**1**, **2a** and **3**) confirm the previously reported formation of the XB co-crystal **1·3** in acetone and clearly establish by PXRD that it is the sole product under the experimental conditions used (Fig. 2). The experiments in the other six solvents, however, establish the pivotal role of the solvent in determining the outcome of the competition between halogen bonding and hydrogen bonding in the self-assembly process that leads to co-crystal formation. The XB co-crystal also forms exclusively in the three solvents more polar than acetone, but decreasing the solvent polarity increases the likelihood of formation of the HB network **2a·3**, such that mixtures of the two co-crystals are formed in CHCl_3 and CH_2Cl_2 , but the HB network is formed exclusively in toluene (Table 1, Fig. 3).



Table 1 Outcomes of competitive co-crystallization experiments, as established by PXRD, in all solvents, listed in order of increasing polarity^a

| Solvent | $E_T(30)$ | System A (1, 2a, 3) | System B (1, 2b, 3) | System C (1, 2c, 3) |
|--------------------|-----------|------------------------|------------------------|------------------------|
| Toluene | 33.9 | HB | HB | HB |
| Chloroform | 39.1 | Mixed HB/XB | HB | HB |
| Dichloromethane | 40.7 | Mixed HB/XB | Mixed HB/XB | HB |
| Acetone | 42.2 | XB | XB | HB |
| Acetonitrile | 45.6 | XB | XB | HB |
| Nitromethane | 46.3 | XB | XB | HB |
| <i>i</i> -Propanol | 48.4 | XB | XB | Mixed HB/XB |

^a Solvent polarity lacks a formal quantitative IUPAC definition and is rather a loosely defined term that encompasses a number of solvent properties. We have used the Reichardt $E_T(30)$ parameter,⁴⁰ which is one of the most commonly used quantitative representations of the solvent properties associated with the concept of solvent polarity. HB refers to hydrogen-bonded co-crystal 2a·3 (system A), 2b·3 (system B) or 2c·3 (system C); XB refers to halogen-bonded co-crystal 1·3.

The outcomes from systems B and C establish the generality of the findings (Table 1). Thus, increasing the HB donor strength by changing from 2a to 2b results in formation of the HB co-crystal (now 2b·3) becoming more probable in increasingly polar solvents. Thus, formation of 2b·3 occurs almost exclusively (HB \geq 95%) in all solvents less polar than acetone, whereas the XB co-crystals 1·3 form exclusively in acetone and the more polar solvents. Further increase in the HB donor strength by using 2c leads to formation only of the HB co-crystal

(2c·3) in all solvents except *i*-propanol, the most polar solvent used, in which a mixture of the HB and XB co-crystals results, with former dominating.

In parallel to the diffraction studies of co-crystal formation, the strengths of the hydrogen bonding and halogen bonding interactions present in the co-crystals were examined in solution by NMR spectroscopic titration. In order to limit the solution-phase studies to 1 : 1 binding and to ensure solubility at the concentrations needed, monoprotic analogues of 1–3 were used for the titrations (C_6F_5I for 1; *p*-cresol for 2a, 2-fluoro-*p*-cresol and 3-fluoro-*p*-cresol for 2b, C_6F_5OH for 2c, and 4-picoline for 3). Titrations were carried out in three of the seven solvents used for the co-crystallization experiments, toluene, chloroform and acetonitrile and the changes in 1H and/or ^{19}F chemical shifts were fitted to 1 : 1 binding isotherms, enabling association constants for the hydrogen bonding or halogen bonding interaction to be determined (Table 2). The titrations establish that monofluorination of the phenol leads to a small increase in association constant and perfluorination leads to a more dramatic increase, for titrations in a given solvent, confirming the increase in hydrogen bond donor capability from 2a to 2b to 2c, with the greater change being from 2b to 2c. Association constants for all hydrogen bonds decrease with increasing solvent polarity from toluene to chloroform to acetonitrile. It is also noted that the association constants for the halogen-bonded complexes are effectively too small to measure in all three solvents. These association constants are smaller than those of all hydrogen bonds in toluene and chloroform and any change in halogen bond strength upon increasing solvent polarity cannot be discerned.

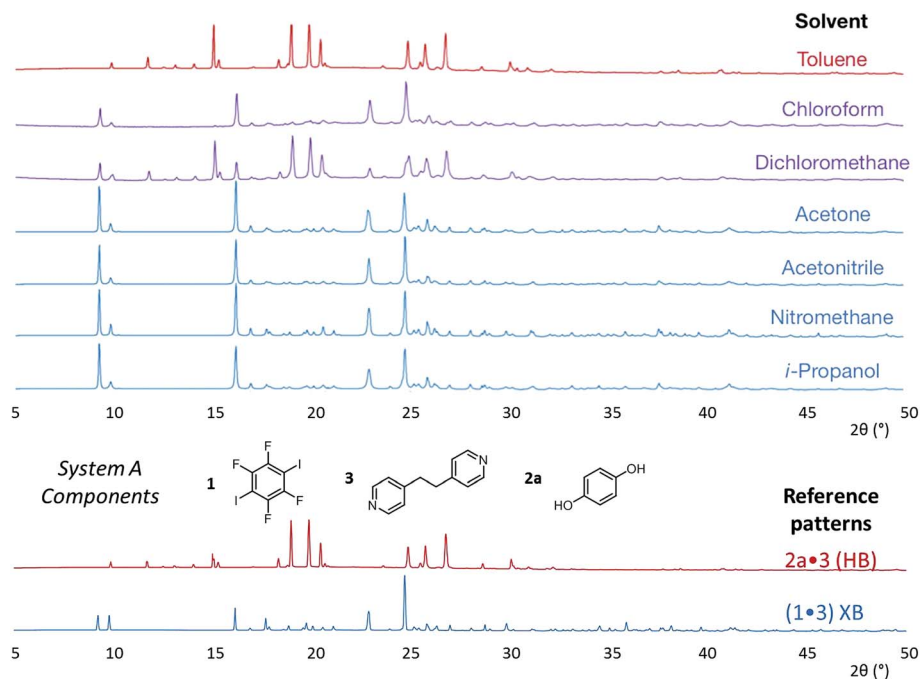
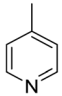
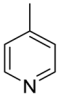
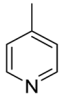
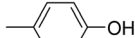
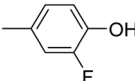
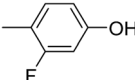
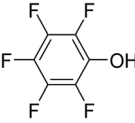
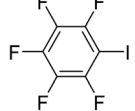


Fig. 3 Powder X-ray diffraction patterns for products of system A competitive co-crystallizations from 7 solvents. Patterns shown in red when only HB co-crystals were formed, blue when only XB co-crystals were formed and purple when mixtures of HB and XB co-crystals were detected. All patterns are shown in the range $17.7 \text{ \AA} > d > 1.82 \text{ \AA}$. For clarity of presentation, the scales are adjusted to allow representation as 2θ ($^\circ$) appropriate for Cu-K α radiation. Fits to patterns are provided in Section 10 of ESI.†



Table 2 Association constants (M^{-1}) from NMR spectroscopic titrations at 298 K^a

| Solvent | Toluene | Chloroform | Acetonitrile |
|---|---|---|---|
| Guest |  |  |  |
| Host | | | |
|  | 31 ± 1 | 19 ± 2 | <1 |
|  | 40 ± 1 | 20 ± 1 | <1 |
|  | 62 ± 5 | 52 ± 2 | <1 |
|  | 1300 ± 50 | 850 ± 60 | 19 ± 1 |
|  | 1 ± 1 | <1 | <1 |

^a Errors determined by 2 × standard deviation of multiple repeat titrations.

The solution-phase interactions require the formation of the HB or XB and the desolvation of the interacting functional groups. Co-crystal formation also requires formation of the HB or XB, but involves desolvation of the entire molecule and formation of additional intermolecular interactions, such as stacking of the aromatic rings and C–H...O hydrogen bonds. Kinetics effects may also play a role in the co-crystal competition experiment, whereas the solution-phase measurements are made at thermodynamic equilibrium. Thus the solution-phase bimolecular association and the co-crystal formation have important common features, but are not identical. Our measurements show the importance of the solvent in determining the strength of interaction in solution and the type of co-crystal formed. They show that solvent polarity has a major effect on the outcome of co-crystallization experiments. More polar solvents weaken HB interactions in solution and favour XB co-crystals.

The boundary between HB and XB co-crystal formation shifts to higher polarity solvents as the HB interaction energy increases, and the solution-phase HB and XB association constants are consistent with this outcome. Thus, in toluene solution the association constants for hydrogen bonding are maximised and are stronger than halogen bonding for all three HB donors, which is consistent with the fact that only HB co-crystals are observed from this solvent. The solution-phase association constants are much lower in acetonitrile, so that

only the stability of the hydrogen-bonded complex with the perfluorinated phenol could be measured. This result is again in agreement with the observation of HB co-crystals for the competition experiment with perfluorinated hydroquinone **2c** in acetonitrile. In chloroform solution, hydrogen bonding is stronger than halogen bonding for all three HB donors, and HB co-crystals are formed for all three HB donors in this solvent. The solution-phase association constants are consistent with the outcome of the co-crystal competition experiment in chloroform, but in the case of hydroquinone some XB co-crystals are also observed. The consistency between solution-phase measurements and co-crystal formation indicates that the HB/XB are the dominant intermolecular interactions in determining the outcome of the co-crystal competition experiment. The only discrepancy is the system **A** result in chloroform, which shows that the other factors do have some influence on the crystallization outcome.

Previous studies of competition between hydrogen bonding and halogen bonding in co-crystal formation^{37,41–43} have focused on tuning halogen bond strength, which is often empirically estimated or qualitatively ranked rather than quantified. In all prior studies the role of solvent has not been taken into account. In most cases a single crystallization solvent has been used exclusively, or at least predominantly, this solvent often being an alcohol or acetone. In the very few studies that consider the role of solvent, focus is restricted to solution-phase binding^{15,36,44,45} and does not consider the impact on controlling crystallization, but supports the potentially important role for halogen bonding in more polar solvents.

Conclusions

We have demonstrated the critical role of solvent in directing self-assembly by examining a system in which either hydrogen bonding or halogen bonding may play a prominent role and showing that either hydrogen-bonded co-crystals or halogen-bonded co-crystals can be selected exclusively by appropriate choice of solvent. The role of solvent choice has been evaluated experimentally in seven solvents using molecular components that are representative of commonly used molecular building blocks in supramolecular systems. All products have been identified and their phase purity or composition determined by analysis of powder X-ray diffraction data. Specifically, hydrogen-bonded co-crystals form in the least polar solvents and halogen-bonded co-crystals in the more polar solvents. The solvent polarity at which the preference switches from hydrogen bonding to halogen bonding depends upon the relative strength of the two types of interaction. The influence of solvent is all the more striking because it is not immediately evident that halogen bonds should be favoured in the more polar solvents.

The implications of the results are not restricted to the development of co-crystals, which are seen as a practical option for tuning the physical properties of the solid forms of the active ingredients of pharmaceuticals, agrochemicals, high-energy-density materials (*e.g.* explosives & propellants), and other molecular crystalline materials. The results point to the wider importance of understanding solvation in the context of



numerous physical and chemical phenomena,⁴⁶ most directly those involving self-assembly and molecular recognition, but encompassing areas such as materials chemistry, catalysis and ion transport and recognition. We believe the results will stimulate examination of solvent-control of intermolecular interactions in many of these areas of application.

Experimental section

¹H and ¹⁹F NMR spectroscopic titrations

¹H and ¹⁹F NMR spectra were recorded on a Bruker Avance II 400 spectrometer at 400.1 MHz and 374.9 Hz respectively at 298 K, using the residual proton signal of the deuterated solvent or a capillary insert with D₂O as the reference. For ¹H NMR spectra, the chemical shifts (δ_{H}) are assigned relative to tetramethylsilane (TMS) at $\delta_{\text{H}} = 0$. For ¹⁹F NMR spectra, the chemical shifts (δ_{F}) are assigned relative to CFCl₃ at $\delta_{\text{F}} = 0$. Analyses of NMR spectra were carried out using Topspin version 3.2 or iNMR version 5.2.1. Measurement of mass of solids was carried out on a Precisa 125A balance. Measurement of volumes of liquids was carried out using Eppendorf Multipette XStream electronic pipettors. In a typical titration 10 Norell S-400 NMR tubes, each with different concentrations of host and guest as measured with a programmed Multipette XStream, were used to record NMR spectra using the automated sample recording system (BACS). The concentration of guest (4-picoline) was chosen to obtain a binding isotherm of >50% saturation in each titration. Titrations were repeated at least twice for reproducibility and estimation of errors. Binding constants, K_{a} , were determined by non-linear least-squares fitting the observed and calculated chemical shifts to a 1 : 1 binding isotherm using a macro-based Microsoft Excel fitting program written by Christopher A. Hunter (University of Cambridge). Where possible fits were conducted using multiple ¹H or ¹⁹F signals for each titration. For further details see ESI section 4.†

Single crystal X-ray diffraction studies of co-crystals

Intensity data for **2b**·**3** and **2c**·**3** were collected at 100 K on either a Bruker SMART APEX-II CCD diffractometer operating with a Mo-K α sealed-tube X-ray source or Bruker D8 VENTURE diffractometer equipped with the PHOTON 100 CMOS detector, using a Cu-K α microfocus X-ray source. A summary of data collection and structure refinement parameters is provided in the ESI (Table S3†). Data were corrected for absorption using empirical methods (SADABS) based upon symmetry equivalent reflections combined with measurements at different azimuthal angles.⁴⁷ The crystal structures were solved and refined against all F^2 values using SHELXL⁴⁸ accessed via the Olex2 program.⁴⁹ Non-hydrogen atoms were refined anisotropically. Hydrogen atoms were placed in calculated positions with idealized geometries and then refined by employing a riding model and isotropic displacement parameters. Crystal structures of **1**·**3** and **2a**·**3** have been previously reported and are therefore not reported in full here.³⁷

Powder X-ray diffraction studies

Microcrystalline powder samples were loaded into 0.7 mm borosilicate capillaries. X-ray diffraction data were collected using

either synchrotron radiation at beamline I11 at Diamond Light Source⁵⁰ or at the University of Sheffield using Cu-K α radiation on a Bruker D8 ADVANCE X-ray powder diffractometer equipped with focusing Göbel mirror optics and a high-resolution energy-dispersive Lynxeye XE detector. Full details of data collections are provided in ESI.† Powder pattern indexing and fitting was carried out using the TOPAS program.^{51,52} Where the powder pattern could be indexed as a single phase, the phase purity of the material was established by Pawley refinement³⁸ and where a mixture of products was identified upon indexing, mixed-phase Rietveld refinement³⁹ was conducted to establish the relative proportions of the products. Comparison with powder patterns calculated from single crystal structures was used to provide a preliminary qualitative assessment of experimental powder patterns prior to quantitative fitting. Full details of fitting of powder patterns are provided in Sections 8–12 of the ESI.†

Acknowledgements

This work was supported by the EPSRC (EP/J012955/1 and EP/J012998/1) and by the University of Sheffield. We are grateful to Diamond Light Source for provision of beam time at beamline I11.

Notes and references

- 1 J.-M. Lehn, *Angew. Chem., Int. Ed. Engl.*, 1990, **29**, 1304–1319.
- 2 *Supramolecular Chemistry: From Molecules to Nanomaterials*, ed. P. A. Gale and J. W. Steed, Wiley, Weinheim, 2012.
- 3 G. R. Desiraju, J. J. Vittal and A. Ramanan, *Crystal Engineering: a Textbook*, World Scientific Publishing Co., Singapore, 2011.
- 4 C. B. Aakeröy, N. R. Champness and C. Janiak, *CrystEngComm*, 2010, **12**, 22–43.
- 5 T. Aida, E. W. Meijer and S. I. Stupp, *Science*, 2012, **335**, 813–817.
- 6 S. Das, G. W. Brudvig and R. H. Crabtree, *Chem. Commun.*, 2008, 413–424.
- 7 G. Cavallo, P. Metrangolo, R. Milani, T. Pilati, A. Priimagi, G. Resnati and G. Terraneo, *Chem. Rev.*, 2016, **116**, 2478–2601.
- 8 L. C. Gilday, S. W. Robinson, T. A. Barendt, M. J. Langton, B. R. Mullaney and P. D. Beer, *Chem. Rev.*, 2015, **115**, 7118–7195.
- 9 L. Brammer, G. Mínguez Espallargas and S. Libri, *CrystEngComm*, 2008, **10**, 1712–1727.
- 10 K. Rissanen, *CrystEngComm*, 2008, **10**, 1107–1113.
- 11 F. Zordan, L. Brammer and P. Sherwood, *J. Am. Chem. Soc.*, 2005, **127**, 5979–5989.
- 12 C. B. Aakeröy, M. Baldrighi, J. Desper, P. Metrangolo and G. Resnati, *Chem.–Eur. J.*, 2013, **19**, 16240–16247.
- 13 L. Meazza, J. A. Foster, K. Fucke, P. Metrangolo, G. Resnati and J. W. Steed, *Nat. Chem.*, 2012, **5**, 42–47.
- 14 M. R. Scholfield, C. M. Vander Zanden, M. Carter and P. S. Ho, *Protein Sci.*, 2013, **22**, 139–152.
- 15 M. J. Langton, S. W. Robinson, I. Marques, V. Félix and P. D. Beer, *Nat. Chem.*, 2014, **6**, 1039–1043.



- 16 A. Vargas Jentzsch, D. Emery, J. Mareda, S. K. Nayak, P. Metrangolo, G. Resnati, N. Sakai and S. Matile, *Nat. Commun.*, 2012, **3**, 905.
- 17 F. Kniep, S. H. Jungbauer, Q. Zhang, S. M. Walter, S. Schindler, I. Schnapperelle, E. Herdtweck and S. M. Huber, *Angew. Chem., Int. Ed.*, 2013, **52**, 7028–7032.
- 18 A. Priimagi, G. Cavallo, P. Metrangolo and G. Resnati, *Acc. Chem. Res.*, 2013, **46**, 2686–2695.
- 19 T. Shirman, R. Kaminker, D. Freeman and M. E. van der Boom, *ACS Nano*, 2011, **5**, 6553–6563.
- 20 P. Politzer, J. Murray and T. Clark, *Phys. Chem. Chem. Phys.*, 2010, **12**, 7748–7757.
- 21 P. Vishweshwar, J. A. McMahon, J. A. Bis and M. J. Zawarotko, *J. Pharm. Sci.*, 2006, **95**, 499–516.
- 22 N. Qiao, M. Li, W. Schlindwein, N. Malek, A. Davies and G. Trappitt, *Int. J. Pharm.*, 2011, **419**, 1–11.
- 23 B. S. Sekhon, *Int. J. Agrochem. Plant Prot.*, 2014, **2**, 44–47.
- 24 D.-K. Bučar, S. Filip, M. Arhangeliskis, G. O. Lloyd and W. Jones, *CrystEngComm*, 2013, **15**, 6289–6291.
- 25 O. Bolton, L. R. Simke, P. F. Pagoria and A. J. Matzger, *Cryst. Growth Des.*, 2012, **12**, 4311–4314.
- 26 C. B. Aakeröy, T. K. Wijethunga and J. Desper, *Chem.–Eur. J.*, 2015, **21**, 11029–11037.
- 27 M. C. Etter, *J. Phys. Chem.*, 1991, **95**, 4601–4610.
- 28 M. Habgood, M. A. Deij, J. Mazurek, S. L. Price and J. H. ter Horst, *Cryst. Growth Des.*, 2010, **10**, 903–912.
- 29 H. C. S. Chan, J. Kendrick, M. A. Neumann and F. J. J. Leusen, *CrystEngComm*, 2013, **15**, 3799–3807.
- 30 P. A. Wood, N. Feeder, M. Furlow, P. T. A. Galek, C. R. Groom and E. Pidcock, *CrystEngComm*, 2014, **16**, 5839–5848.
- 31 F. H. Allen, *Acta Crystallogr., Sect. B: Struct. Sci.*, 2002, **58**, 380–388.
- 32 L. Zhao, V. Raval, N. E. B. Briggs, R. M. Bhardwaj, T. McGlone, I. D. H. Oswald and A. J. Florence, *CrystEngComm*, 2014, **16**, 5769–5780.
- 33 M. D. Eddleston, B. Patel, G. M. Day and W. Jones, *Cryst. Growth Des.*, 2013, **13**, 4599–4606.
- 34 C.-Q. Wan, A.-M. Li, S. A. Al-Thabaiti, E.-S. H. El-Mosslamy and T. C. W. Mak, *CrystEngComm*, 2014, **16**, 8960–8968.
- 35 C. A. Hunter, *Angew. Chem., Int. Ed.*, 2004, **43**, 5310–5324.
- 36 C. C. Robertson, R. N. Perutz, L. Brammer and C. A. Hunter, *Chem. Sci.*, 2014, **5**, 4179–4183.
- 37 E. Corradi, S. V. Meille, M. T. Messina, P. Metrangolo and G. Resnati, *Angew. Chem., Int. Ed.*, 2000, **39**, 1782–1786.
- 38 G. S. Pawley, *J. Appl. Crystallogr.*, 1981, **14**, 357–361.
- 39 H. M. Rietveld, *J. Appl. Crystallogr.*, 1969, **2**, 65–71.
- 40 C. Reichardt, *Chem. Rev.*, 1994, **94**, 2319–2358.
- 41 C. B. Aakeröy, C. L. Spartz, S. Dembowski, S. Dwyre and J. Desper, *IUCrJ*, 2015, **2**, 498–510.
- 42 G. Mínguez Espallargas, F. Zordan, L. Arroyo Marín, H. Adams, K. Shankland, J. van de Streek and L. Brammer, *Chem.–Eur. J.*, 2009, **15**, 7554–7568.
- 43 T. Shirman, M. Boterashvili, M. Orbach, D. Freeman, L. J. W. Shimon, M. Lahav and M. E. van der Boom, *Cryst. Growth Des.*, 2015, **15**, 4756–4759.
- 44 M. G. Sarwar, B. Dragisic, L. J. Salsberg, C. Gouliaras and M. S. Taylor, *J. Am. Chem. Soc.*, 2010, **132**, 1646–1653.
- 45 Q.-Z. Li, B. Jing, R. Li, Z.-B. Liu, W.-Z. Li, F. Luan, J.-B. Cheng, B.-A. Gong and J.-Z. Sun, *Phys. Chem. Chem. Phys.*, 2011, **13**, 2266–2271.
- 46 C. A. Hunter, *Chem. Sci.*, 2013, **4**, 1687–1700.
- 47 L. Krause, R. Herbst-Irmer, G. M. Sheldrick and D. Stalke, *J. Appl. Crystallogr.*, 2015, **48**, 3–10.
- 48 G. M. Sheldrick, *Acta Crystallogr., Sect. C: Struct. Chem.*, 2015, **71**, 3–8.
- 49 O. V. Dolomanov, L. J. Bourhis, R. J. Gildea, J. A. K. Howard and H. Puschmann, *J. Appl. Crystallogr.*, 2009, **42**, 339–341.
- 50 S. P. Thompson, J. E. Parker, J. Potter, T. P. Hill, A. Birt, T. M. Cobb, F. Yuan and C. C. Tang, *Rev. Sci. Instrum.*, 2009, **80**, 075107.
- 51 A. A. Coelho, *TOPAS Academic, version 4.1*, 2007, see <http://www.topas-academic.net>.
- 52 A. A. Coelho, J. S. O. Evans, I. R. Evans, A. Kern and S. Parsons, *Powder Diffr.*, 2011, **26**, S22–S25.

